Design of a mechanical loading device for studying the load-dependent transport of solutes across articular cartilage in a micro-CT chamber

Master of Science Thesis

Asimina Glynou

MSc Biomedical Engineering, Tissue Biomechanics and Implants (4245199)
October 2014

Supervisors: Harrie Weinans, Amir Abbas Zadpoor, Behdad Pouran

TU DELFT, Department of Biomechanical Engineering, Faculty of Mechanical, Maritime, and Materials Engineering

Abstract

Articular hyaline cartilage is the smooth shiny avascular tissue that establishes a connection between the joint-forming bones, like tibia and femur for the case of knee joint. Being avascular, articular cartilage relies on specific transport mechanisms to maintain its survivorship. Those mechanisms are strongly related to in-vivo conditions, like loading regimes and electrochemical phenomena. Despite its remarkable load-bearing properties, articular cartilage is prone to degeneration due to its avascularity. Therefore pathological conditions like Osteoarthritis (OA) are very likely to develop, resulting in excessive pain and respectively in restriction of the patient's normal daily activities. It has been shown that the study of the aforementioned transport mechanisms is an indication of the tissue integrity. Additionally tissue engineering approaches are focusing on the optimization of the transport parameters that derive the functionality of articular cartilage. Many studies have focused on the study of solutes transport under loading conditions, i.e. *convection,* with techniques like fluorescent microscopy. Accordingly, imaging modalities like Contrast Enhanced Computed Tomography (CECT) and MRI have been employed to determine the tissue integrity by studying transport mechanisms that are correlated to electrical phenomena. However, a setup that would allow convection studies in a clinical tool like a CT scanner has not been developed yet. In the present study, for the first time a novel mechanical loading device that facilitates the load-dependent transport of solutes across articular cartilage in a micro-CT chamber has been developed and validated. The work aims at unraveling the optimal conditions under which viable tissue constructs could be created, and if successful it can constitute a powerful clinical tool towards the permanent treatment of cartilage related diseases. The machine allows to compress various tissue plugs under various loading regimes as well as to monitor the applied forces simultaneously. The validation was performed with respect to (i) accurate contact of the indenters with the cartilage, (ii) accurate mechanical response and (iii) the functional operation of the device in the micro-CT chamber. The validation process highlighted the successful operation of the device upon service, and it indicated its further incorporation in the convection experiments. Additionally, it was proved that the device allows to monitor the mechanical properties of soft materials at high accuracy levels. The Contrast Enhanced Computed Technique (CECT) was implemented in order to determine the penetration levels of the solutes across articular cartilage; for this specific purpose the

neutral contrast agent VISIPAQUE, was used and images were taken at discrete time points. The results show increased penetration of the contrast agent upon application of the loading pattern. However the statistical significance of the results could not be proved, partially due to variations between the geometry of the samples as well as the experimental conditions. Nevertheless, the validation together with the experiments proved the potential of the device to be successfully used for the particular cause. On the other hand more investigation is needed in order to obtain a well-established outcome, which will support the beneficial effect of the specific loading pattern on the biological response of cartilage.

1. Introduction

Articular cartilage is a load bearing tissue that covers the ends of synovial joints as shown in figure 1. Articular cartilage allows the smooth performance of the daily activities and it ensures reduced friction upon movement (Mow et al. (1992) Pearle et al.,(2005)). Being avascular, it performs its metabolic activities, i.e. nutrition and disposal of wastes via specific transport routes: (i) surrounding synovial fluid (primarily) and (ii) subchondral bone. The primary transport mechanism is diffusion of the solutes down to the chemical potential gradient, which is termed *Fickean diffusion* (Schulz and Bader, 2007) and is described by Fick's law of diffusion: $\vec{\Gamma} = -D\nabla c$.

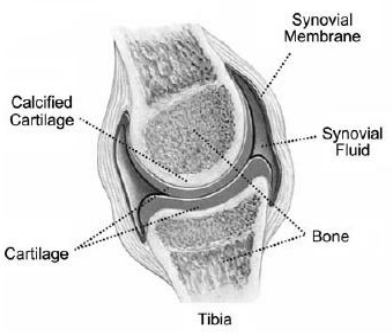

Figure 1: Articular cartilage in the knee joint (Schulz and Bader, 2007).

The solid matrix of articular cartilage consists mainly of Collagen II and negatively charged Glycosaminoglycans (GAGs), while the fluid phase consists of water and mobile ions (see figure 2). To maintain electro-neutrality condition in the cartilage, GAGs attract mobile ions from the surrounding fluid into the matrix that gives rise to enhanced cartilage's water content. This phenomenon causes the cartilage to resist external compressive loads (Lai et al., 1993, Ateshian et al., 1997, Mow et al., 1992). The electric phenomenon then introduces another diffusion type, which is widely recognized as the *Non-Fickean diffusion.*

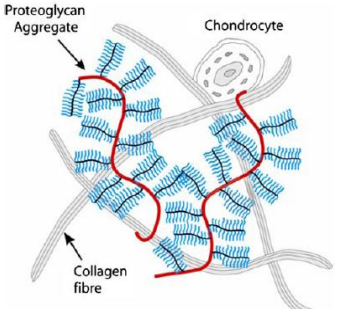

Figure 2: The structure of cartilage(Schulz and Bader, 2007).

Apart from its distinct biochemical composition, articular cartilage is characterized by a prevalent depth-varying structural organization into the superficial zone, middle zone, deep zone and the calcified cartilage zone, as illustrated in figure 3. The superficial zone accounts for about the 10%-20% of the cartilage thickness and it is occupied by chondrocytes that secrete a relatively low amount of proteoglycans. As far as the collagen network is concerned, it consists of collagen fibers that are oriented in parallel to the surface (Schulz and Bader, 2007). On the other hand, the middle zone is thicker (40%-60% of the tissue depth) and it consists of chondrocytes that secrete a higher

amount of proteoglycans. Additionally to this, collagen fibers are oriented obliquely to the surface, while they are also shown to be thicker.

The deep layer is characterized by the presence of rounded chondrocytes, high proteoglycan content and also by a radically oriented collagen network. Finally, the calcified zone is the junction between the cartilage tissue and the subchondral bone; it is separated from the deep zone by a tidemark zone shown in (Poole C. A, 1992)**.** The calcified zone contains small rounded chondrocytes, but proteoglycans are not present within the ECM. The collagen matrix in this zone is composed of radically oriented collagen fibers anchored in a calcified matrix (Poole, 1997, Pearle et al., 2005, Schulz and Bader, 2007, Sophia Fox et al., 2009).

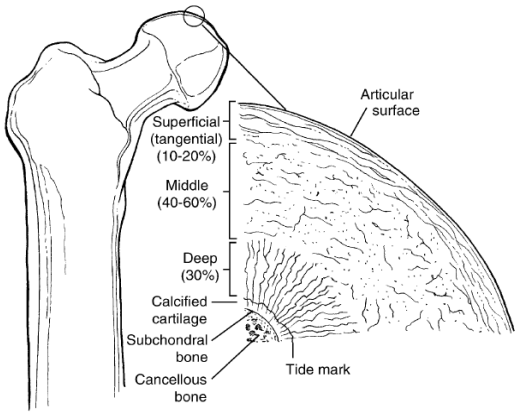

Figure 3:Articular Cartilage zonal structure (Pearle et al., 2005).

The particular biochemical composition and the structural arrangement of articular cartilage make it capable of resisting large loads of several times the body weight upon various daily activities (Poole, 1997, Pearle et al., 2005). Typically, the hip and the knee joint , which are the major load bearing joints found in the human body, may withstand forces up to 10 times the body weight during daily activities, like walking, rising from a chair or climbing (Mow et al., 1992). Articular cartilage is subjected to a complex loading pattern that involves tension, compression, shear stresses and hydrodynamic pressure. However, compression appears to be the most significant mechanical stimulus encountered within the articular cartilage (Mow et al., 1992), something that is also

supported by studies focusing on the effects of the aforementioned stimuli on cartilage's metabolism (Heath and Magari, 1996).

With respect to the compressive strains that are encountered within the tissue, the average compression amplitudes are found to be more than 13% for movements like walking (Schulz and Bader, 2007), a result that is also supported by Armstrong and his group (Armstrong et al., 1979). Specifically Armstrong and his colleagues conducted experiments in articular cartilage of femoral heads in order to determine the deformation under an applied load of five body weights; their finding showed non-uniformly distributed compressive strains of amplitude equal to 15%-20%, which were age dependent. Upon application of the aforementioned loading regimens, the previously described electric phenomena in cartilage associate with induced fluid motion that can considerably affect the solute transport; this induced transport is called *convection* and is described as the sum of diffusive and convective contributions: $\vec{\Gamma} = -D\nabla c + \omega c\vec{U}$, where ω the convection coefficient and U the average velocity of the moving quantity.

The behavior of articular cartilage under loading conditions has been often studied based on the so-called *biphasic* model, due to the known interaction of the solid phase with the fluid phase (Mow et al., 1984, Guilak and Mow, 2000). However, articular cartilage is highly inhomogeneous due to the presence of the layers and zones described previously. Furthermore, the variation in the orientation of the collagen fibers within solid matrix, result in a highly anisotropic response to mechanical stimulation. The flow of the fluid phase upon loading and the presence of both collagen fibers and proteoglycans within the matrix of the tissue, result in viscoelastic material properties (Mow et al., 1992).

Just like with every material, the response of articular cartilage is described by specific materials properties, like the aggregate modulus, Young's modulus, and shear modulus. Aggregate modulus, which can be estimated be subjecting tissue samples to confined compression, is defined as the measure of stiffness of the tissue when fluid flow has completely ceased. Evaluation of the aggregate modulus is performed by confined compression experimental setups that place the sample in a confided chamber and involve a porous indenter that allows free fluid flow (Boschetti et al., 2004). Typical values of the aggregate modulus were demonstrated by Athanasiou and his group (Athanasiou et al., 1991) for cartilage samples taken from human, bovine, dog, monkey

and rabbit tissue; the values were found to be in the range of 0.5-0.9MPa. Young's modulus can be estimated by unconfined compression tests, and it has been found to vary within the range of 0.45-0.80MPa, while the shear modulus ranges from 0.20-0.40MPa (Mow et al., 1992); typical confined and unconfined compression setups are shown in figure 4.

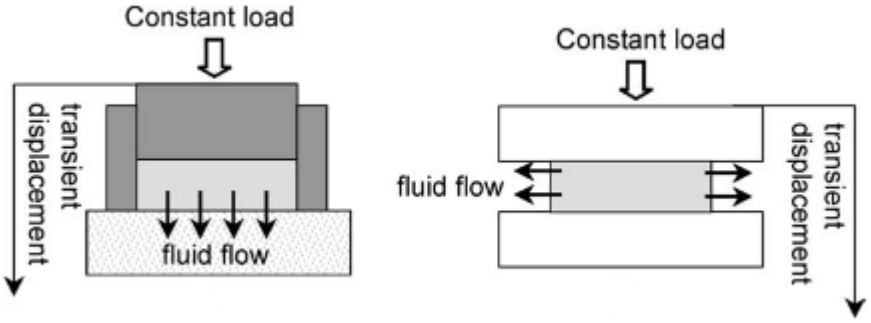

Figure 4: Left: Confined compression setup, right: Unconfined compression setup (Boschetti et al., 2004).

Despite its remarkable properties, articular cartilage can undergo severe alterations in its biochemical and mechanical properties, a condition that is well known as Osteoarthritis (OA). Particularly Osteoarthritis causes the cartilage to develop disturbed mechanical properties, disrupted collagen fibril orientation as well as GAGs depletion. A number of approaches have been developed towards the repair of articular cartilage's defects. The conventional technique consists in the extraction of the articular cartilage and the surrounding bone, followed by the implantation of a metallic prosthesis that aims at the restoration of joint mobility.

Next to that, revolutionary tissue engineering techniques approaches that aim at the generation of tissue constructs have captured the eye of attention the last decades. Tissue engineering methods incorporate cultivation of cells (Mesenchymal stem cells or chondrocytes depending on the medical application) in appropriate scaffold materials that provide a 3D framework for cell growth and attachment. The desired outcome of

those techniques is the production of tissue constructs with biochemical and mechanical properties comparable to those of the native cartilage; that way after their implantation they will take over the function of native tissue contributing that way to a more physiological restoration of the joint mobility.

Modern tissue engineering involves cells culturing in physiologically relevant conditions from the perspective of nutrients transport and compressive loading regimes. The effect of loading conditions has been studied extensively, through the development of Bioreactors that facilitate cells culture under compression regimens (Mauck et al (2000a) Villanueva et al. (2008) Wernike et al. (2008)). One of the most widely used bioreactors, capable of applying intermittent compression (10%, 1Hz) to chondrocyte seeded constructs is illustrated in figure 5; upon the specific loading regime there was a significant improvement of the constructs material properties, while the chondrocytes secreted increased amounts of Collagen II and proteoglycans in a time dependent manner.

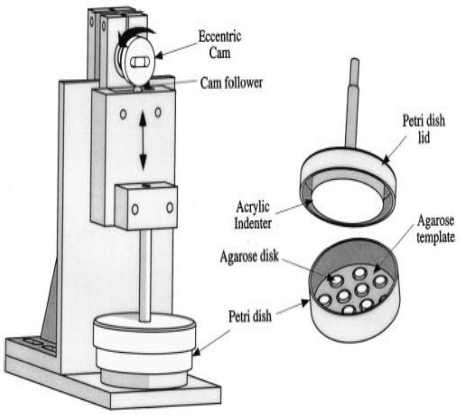

Figure 5: Compressive Bioreactor applying intermittent mechanical stimulation by Mauck et al. (2000).

Next to that, the establishment of the optimal transport conditions has received increased attention as well. Mauck and his colleagues, (Mauck et al., 2003) established a theoretical frame that highlights the role of loading in the transport mechanisms that take place in the cartilage. Based on this study, Albro and his group examined the role of cyclic compression (±5%, 1Hz, 40 hours) on agarose samples that were immersed in DEXTRAN solutions of varying molecular weight. For that reason they developed a custom-made loading device that allowed subjection of the samples to the aforementioned loading regimen. They highlighted a dramatic increase of solutes transport upon the specific loading pattern comparing to the corresponding passive experiments (Albro et al., 2008).

Additionally, Evans and Quinn investigated the influence of dynamic compression on convection coefficients, when subjecting DEXTRAN-immersed bovine osteochondral plugs to 10%-50% ramp profile and consequent release. The technique implemented in

order to evaluate the results was fluorescent microscopy; therefore a custom-made loading device that included a microscope stage was developed. The study highlighted the beneficial role of the specific loading conditions on the convection coefficient and consequently on the metabolic response of the cartilage (Evans and Quinn, 2006). On the other hand, Quinn and his colleagues demonstrated decreased diffusivity of DEXTRAN solutes across bovine explants when subjected to 8%-23% static compression (Quinn et al., 2001). This result was found to be in good correlation with a number of tissue engineering studies that indicated that static compression is associated with a decrease in the metabolic activities of cartilage (Wong et al. (1997), Valhmu et al. (1998)).

Next to the improvement of the existing therapies and approaches, focus has been given on the establishment of effective and fast diagnostic techniques. Particularly, studying the non-Fickean diffusion of ions across articular cartilage can potentially determine the tissue integrity and therefore the progress of OA at its early stages. Specifically, MRI and CECT (Contrast Enhanced Computed Tomography) scans have demonstrated cartilage GAG content. Quantification of the penetration rate of negatively charged contrast agents in the cartilage can help identify the degenerated cartilage (Kokkonen et al., 2011b, Kokkonen et al., 2011a, Kulmala et al., 2010).

On the other hand, clinical tools like CECT are not readily available to investigate the convection in articular cartilage. Thus the development of a setup to study the aforementioned transport mechanisms in a CT-scanner would be an essential tool to address clinical issues (i) progression of Osteoarthritis under loading conditions (ii) finding the most effective transport mechanisms that contribute to the maintenance of cartilage. Besides the transport phenomena, determining the mechanical properties of cartilage is an additional way of evaluating its integrity since it demonstrates whether it is healthy or not. Thus, an additional modality that allows monitoring the mechanical properties of cartilage would create an integrated system capable of determining the properties of articular cartilage in healthy and diseased conditions.

The current study aims to investigate the load dependent transport of neutral solutes across cartilage using Contrast Enhanced Computed Tomography (CECT) technique. For this purpose, we designed a novel loading device that efficiently operates in a micro-CT. The methodology followed in order to develop the device that could readily

operate in the micro-CT is described in the next chapter. The models presented here were generated using SOLIDWORKS 2012 STUDENT EDITION. The results with respect to the operation of the device and the associated validation steps are the presented. After that, the experimental procedure followed in order to investigate the loading effects on the solutes transport across cartilage is explained. Thereafter, the results of the experimental session are given, and they are finally followed by the discussion session, in which comments on the whole process are given along with recommendations for future work.

2. Mechanical Loading Device

2.1. Design Background

The basic idea behind the realization of the specific project might seem rather simple and is derived from the literature findings regarding the design of bioreactors and is illustrated in figure 6: A sample positioned within a holder, an indenter that compresses the sample, an actuator that provides the indenter with the desired motion pattern and a load cell for acquiring the applied forces (Mauck et al. (2000) (Démarteau et al., 2003). However, the implementation of CECT technique in a micro-CT for quantifying the effect of loading on the solutes transport made the present project quite challenging, from the perspective of specific additional requirements that had to be fulfilled. From a first insight, the device had to be designed in a way that would ensure high imaging resolution, prevention of beam hardening effect, facile liquid handling and confrontation of the space limitation in the micro-CT. However, additional requirements rose upon the implementation of the steps following for the aforementioned parameters that give rise to even more challenging process. Therefore, the aim of this chapter is to describe the steps to develop a loading machine that can operate efficiently in a micro-CT.

2.1.1. Space limitation but high resolution

As mentioned before, the compression mode of the device consists of an indenter that receives its motion pattern from an actuator mounted on the top of the device frame, as shown in figure 6. In order to maintain a flexible assembly and disassembly of the device, we built up the device from 4 individual plates that were screwed together to form a single structure, as shown in figure 7. We also considered operating at the maximal imaging resolution (FOV=30mm, resolution=60μm) within the Ø100mm cylindrical micro-CT bore as well as further positioning the device on a Ø30mm half-cylindrical holder. It becomes evident that space limitation issue rise, since the

orientation of the device as shown in figure 6 was not feasible, partially due to the fact that this scenario presupposed the incorporation of a tiny actuator.

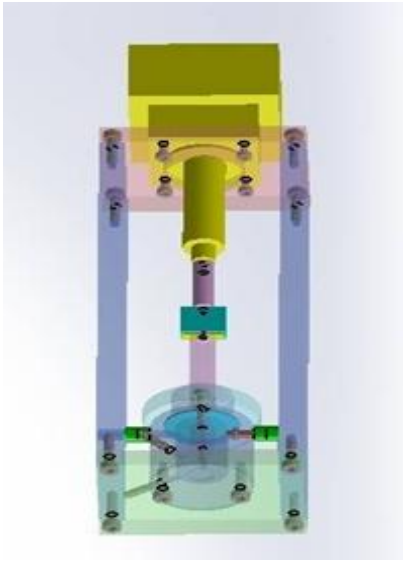

Figure 6: CAD Model: Initial vertical orientation of the device in the micro-CT chamber; the actuator (yellow) is mounted on the top of the device frame.

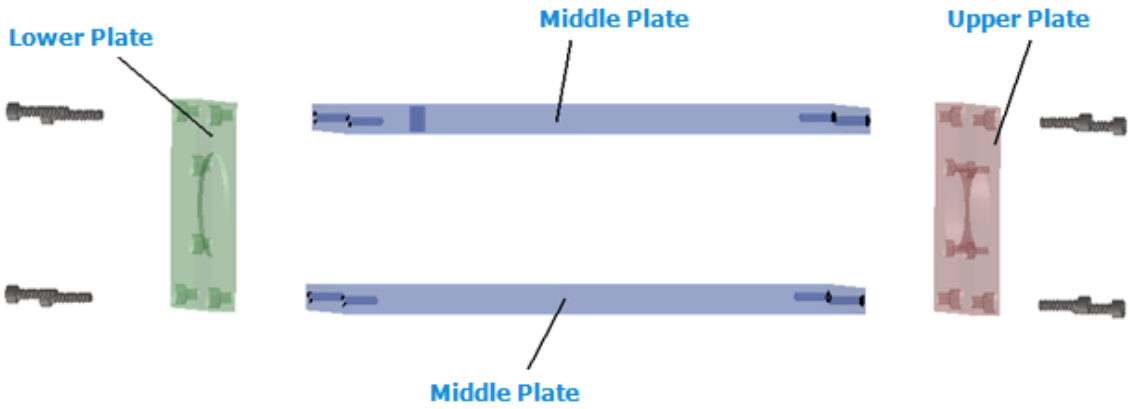

Figure 7: The device frame consisting of four individual plates; the plates are kept together by means of four slotted screws.

In order to overcome the existing space limitation (i) the device was oriented horizontally in the micro-CT as shown in figure 8, (ii) the overall design height was set equal to 8cm and (iii) the minimal possible actuator's height possible was chosen, i.e. 58mm.

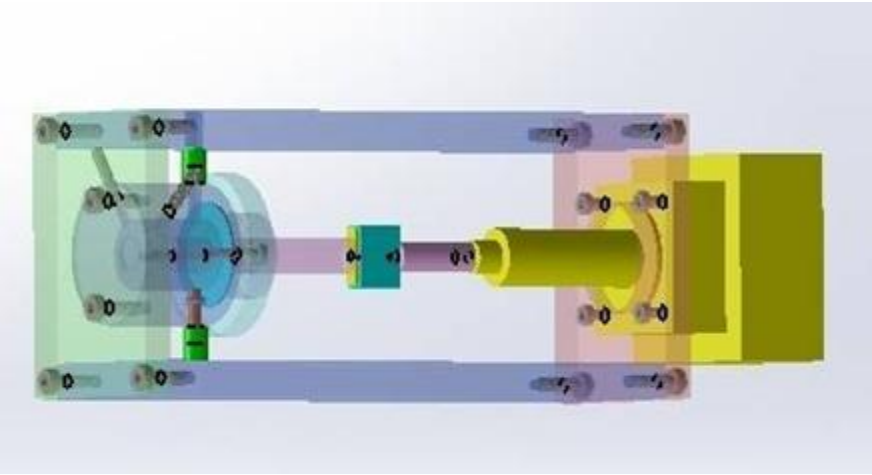

Figure 8: CAD Model: Final horizontal orientation of the device in the micro-CT.

2.1.2. Beam Hardening

The implementation of CECT technique for the purpose of the present work, posed a crucial requirement as far as the choice of the fabrication materials is concerned. Particularly, in order to ensure good imaging quality within the Region of Interest (ROI), scattering effects that could potentially occur due to the hardening of X-Ray beam had to be minimized. The beam hardening effect is very likely to occur when metallic components are present within the ROI; therefore alternative plastic materials had to be chosen for the fabrication of the device components.

Accordingly, we chose a material for the parts that enabled x-ray to pass through it without significant loss of energy. Additionally, a non-hygroscopic material was a priority, due to the fact that the components in direct contact with the contrast agent should remain chemically stable. Last but not least, the plastic material that would

provide superior mechanical and chemical properties should preferably have a reasonable price.

CES EDUPACK 2013**,** a - commercially available software that consists of material libraries was used. A primary comparison between different material candidates with respect to their price versus the compressive strength was performed that is shown in figure 9; among which, thermoplastic Polyvinylchloride (PVC) exhibited good compressive strength with simultaneous low cost per kg. Therefore it was considered as the most suitable candidate. Additionally, when working with plastics, creep is a major issue, since it can adversely affect the reliability of the device performance when the dimensional stability is crucial. PVC is characterized by very well creep properties, which are further enhanced when working in room temperature conditions. Last but not least, PVC is well known for its translucent nature as well as for its non-hygroscopic behavior. Consequently rigid PVC resin (VINK, VINPLAST PVC-U, Polyvinylchloride) was chosen for the manufacturing procedure. Finally, the various parts were connected together by means of Nylon slotted-head screws **(**Nylon PA 6.6 resin).

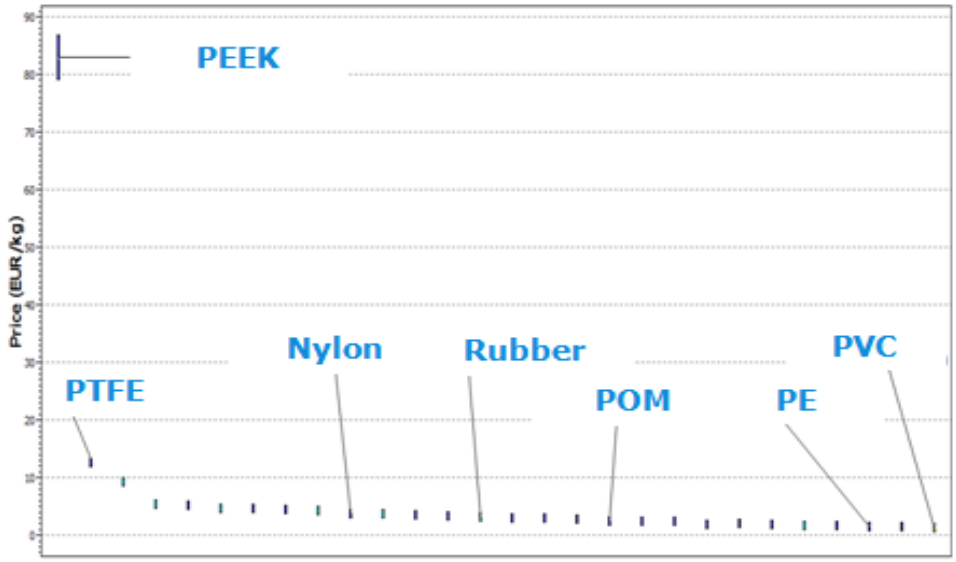

Figure 9: CES EDUPACK 2013 Comparison: Price versus Compressive strength for various polymers.

2.2. Compression unit

2.2.1. Cartilage holder

Equine osteochondral plugs (n=3) were compressed within our loading device; part of the subchondral bone was left in the plugs to mimic the physiological condition and to investigate its contribution to the overall transport mechanism (Bansal et al., 2010, Aula et al., 2009). For the purpose of the particular study the plugs were drilled with a diameter equal to 8.5mm. In order to facilitate the axial diffusion and prevent any radial diffusion effects, the leakage of the contrast agent towards the lateral side of the sample was inhibited (Kokkonen et al., 2011a); therefore the sample was radially wrapped by a thin layer of heat shrinking material (thickness of 0.6mm).

The compression of the plugs took place within a cylindrical chamber, the *cartilage holder*. The holder is capable of allocating one sample per experiment, in a Ø10mm and 2mm deep recess located on the bottom of the holder. In this way we could approach proper positioning and concentric orientation of the sample with respect to the indenter. The capacity of the holder was chosen so that the maximum volume of contrast agent (7ml) or in other words 63 times the cartilage volume could fit. This specific volume was chosen in order to ensure the assumption of infinite baths while keeping scattering effects of X-Ray/contrast agent minimal (Ateshian et al., 2012).

Four slotted screws were additionally used for clamping the sample in order to compensate for the poor stabilization resulting from the horizontal positioning of the device. The holes drilled to recruit the screws clamped only to avoid peripheral damage to the cartilage (see figure 10). Additionally, the heads of each screw was equipped with an O-ring in order to ensure that contrast agent would not leak through these holes (see Appendix A). Besides stabilization of the sample, the holder was also stabilized on the lower plate of the device

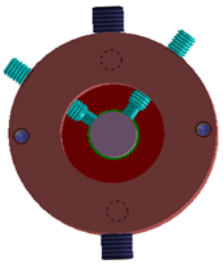

Figure 10: CAD model of the holder; Two out of four sample stabilizing slotted screws.

frame by means of four slotted head screws (see Appendix B). Apart from that, it was positioned in a properly patterned recess in the center of the lower plate, which further enhanced its tight fixation. In addition it ensured its concentric orientation with respect to the indenter (see Figure 11 for details).

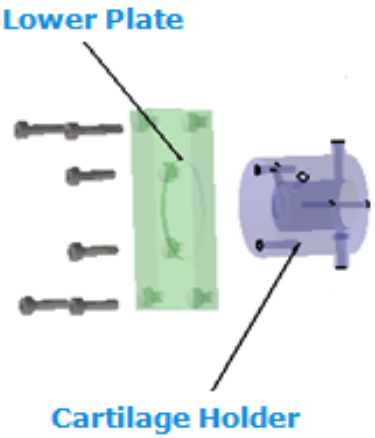

Figure 11: CAD model of the stabilization method followed for the proper positioning of the cartilage holder.

The holder incorporates a reservoir consisting of an upper and a lower channel that allow the addition and the disposal of the contrast agent, respectively. In order to compensate for a possible evaporation of the contrast agent during experiments, both channels are covered with lids. Accordingly, in order to prevent the leakage of the contrast agent towards the lower channel a static seal that consists of a Viton Rubber O-Ring associated with a rod are included (see figure 12). The complete assembly of the holder is shown in figure 13.

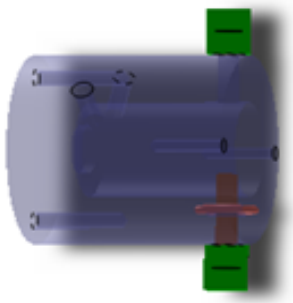

Figure 12: CAD model of the holder: The reservoir for addition/removal of the contrast agent; the static seal consisting of an O-Ring and a rod is additionally illustrated.

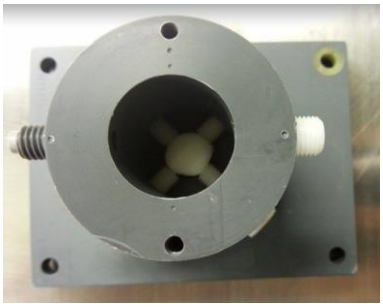

Figure 13: Cartilage holder: Sample shown in the recess, kept in place by four slotted head screws. Additionally: Reservoir consisting from an inlet (right) and outlet (left) port with the static seal.

2.2.2. Leakage-free device operation

The cartilage compression involves the reciprocating movement of an indenter in the holder that is filled with contrast agent. In order to ensure proper horizontal operation of the device we considered a strategy to minimize contrast agent leakage. In preliminary design steps, the leakage-free solution was a dynamic seal consisting of a lid with a groove for positioning of an O-Ring, as shown in figure 14. However, the low penetration speeds that are required for our experimental setup would result in high friction levels between the indenter and the O-ring walls. Therefore, the alternative idea was to incorporate a Ø30mm silicon rubber diaphragm placed on top of the holder. This diaphragm divides the compression unit of the device into two parts: the *inner part* consisting of the holder filled with the contrast agent, the sample and the indenter, and the *outer part* consisting of the components that connect the indenter with the actuator.

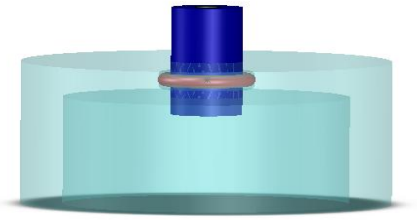

Figure 14: Holder lid including an O-Ring groove; an O-ring would be positioned there and it would prevent leakage phenomena associated with the reciprocating motion of the indenter.

The cylindrical component that ensures the communication of the indenter with the motion system is called *connector* (Ø19mm)*;* the connector and the indenter are clamped by means of a screw that penetrates through the hole of the diaphragm. An annular plate is added on the top of the holder serving two roles: (i) stable positioning of the diaphragm and (ii) guidance of the connector upon movement. The connector is

coupled with a cylindrical *motion rod* that transfers the loading pattern created by the actuator. The load cell is mounted onto the motion rod, before being ultimately connected to the actuator through an additional rod, i.e. the *coupling rod*; the isolated system is further illustrated in the figure 15.

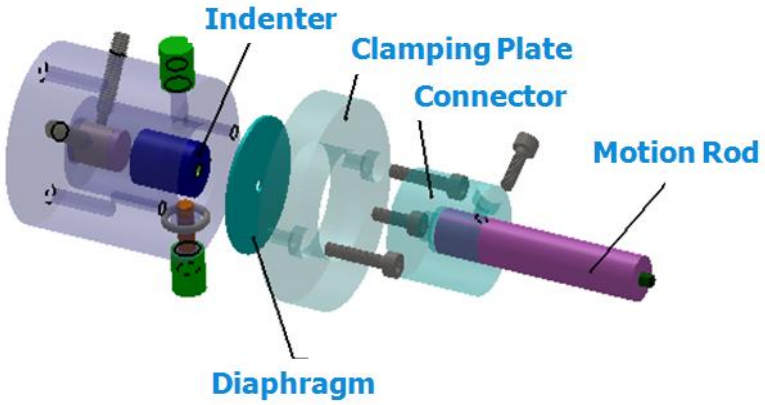

Figure 15: CAD model illustrating the motion unit of the device: The connector, the diaphragm and the cylindrical indenter are kept together with a screw penetrating through the hole of the diaphragm; Connector and motion rod kept as an integrated part by means of a screw.

2.2.3. Indenters

In the present work, the study of the transport phenomena across cartilage surface involved the subjection of the samples to ramp loading regimens. This fact posed specific requirements regarding the design of the indenter. Particularly, the design should allow the continuous fluid and consequently solute exchange between the reservoir and the cartilage during static compression. In order to implement this idea various designs were proposed; either porous structures or micro-channels (see figure 16). With respect to the porosity details, an initial range between 10μm and 500μm was set in accordance with the cartilage tissue engineering literature proposals, for loading platens and scaffolds that enhance the exchange of

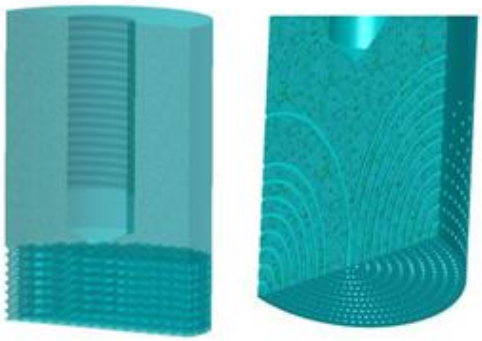

Figure 16: Pores or micro-channels?

nutrients between the surrounding liquid and the samples (Davisson et al., 2002) (Huang et al., 2004, Grad et al., 2006, Jung et al., 2008). The fabrication of indenters with a relatively low pores' size did not seem to be ideal, primarily due to the clogging behavior of the pores that is associated with the choice of plastics for the components of the device. Therefore, a final range for the pores' size within 200μm and 500μm was chosen, and the resulting indenters were tested under service to provide clogging-free operation in the presence of the contrast agent. Thus, the indenters were immersed in VISIPAQUE solution for 24 hours and were scanned afterwards using a micro-CT (Quantum FX, Perkin Elmer, USA) in order to stud the aforementioned clogging potential. Figure 17 depicts that indenters with 200μm average pore size were associated with considerable pore blockage that might potentially inhibit the effective circulation of the contrast agent. As a result indenters with 500μm average pore size were finally chosen for the purposes of the particular study.

Figure 17: Micro-CT images of the indenters; From left to right: (a) 200μm, (b) and (c) 500μm average pore size.

The geometrical details of the indenters, namely the diameter and the length were determined based on specific requirements posed by the experimental setup. Particularly, the diameter was initially set equal to 8.5mm in order to fully cover the surface of the sample. Additionally, eliminating the chance for possible friction between the indenter and the wrapping material was an additional factor that affected the choice of the indenter's diameter. Therefore a second value equal to 7.5mm was chosen and the resulting indenter was validated upon service. However, the aforementioned value was

further reduced, due to the fact that in case of slight misaligned orientation of the sample within the holder's recess resulted in contact of the indenter with the wrapping material. This specific condition led in increased friction levels that obscured the measurements acquired from the load cell; therefore, a final diameter equal to 6.5mm was chosen for the porous indenter.

Additionally, the length of the indenter was chosen based on the reaction force that the silicon rubber membrane exerted upon the displacement: the force required to bring the indenter and the sample into contact. Thus we selected an initial length of 15mm and performed trials with various displacements to record the resulting forces as shown in Table 1 and figure 18. The commanded displacements were prescribed with a velocity equal to 0.15mm/sec, or in other words with the velocity that would be implemented in the later experimental process. Those values along with the height of the cartilage holder and the capacity of the load cell (see Control Unit Section) indicated the length of the indenter.

Table 1 Membrane reaction force for the connector's displacement ranging from [0.1-1.2] mm.

Trial	Displacement (mm)	Average Force (N)	STD (%)
1	0.1	0.233	9
2	0.2	1.059	1.14
3	0.3	2.571	1.24
4	0.4	4.560	1.59
5	0.5	6.548	0.93
6	0.6	8.606	0.28
7	0.7	10.623	1.2
8	0.8	12.268	0.91
9	0.9	13.830	1.52
10	1	15.447	0.57
11	1.1	17.267	1.17
12	1.2	18.962	0.17

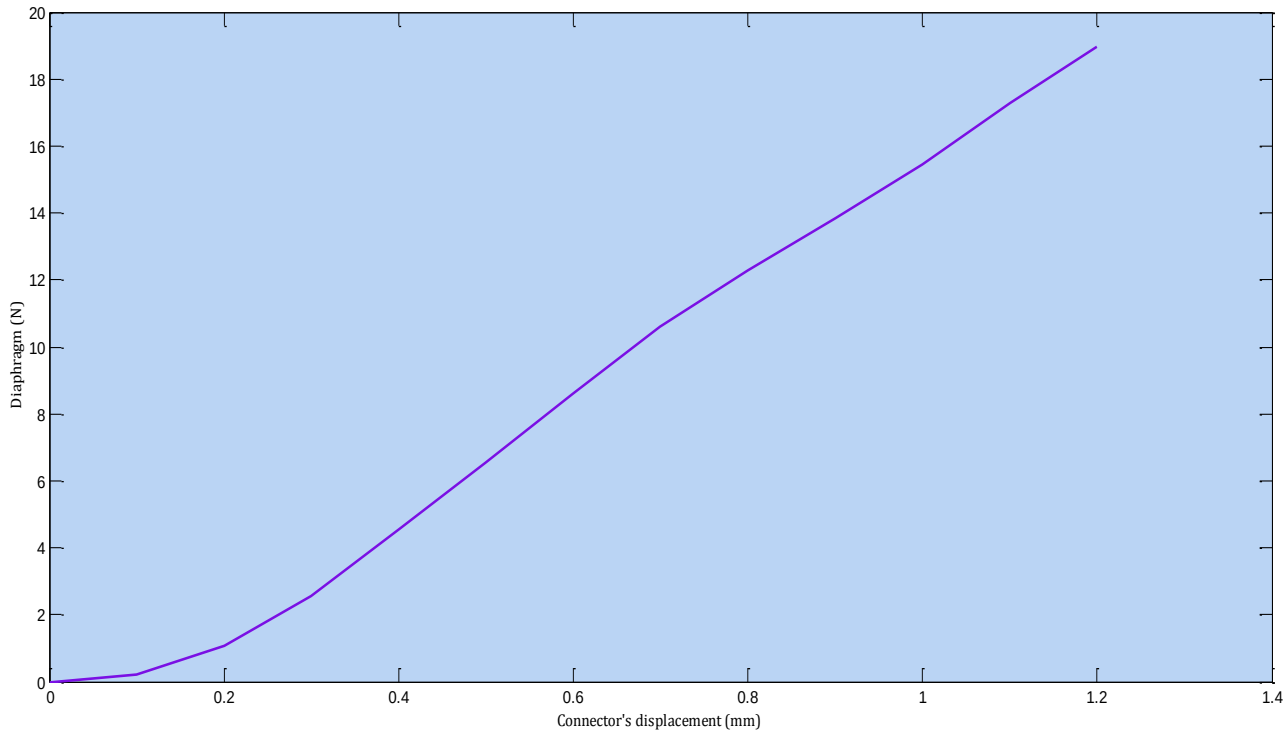

Figure 18: Membrane reaction force versus connector displacement.

For comparison, the behavior of the membrane upon the aforementioned displacement values was studied with a Finite Element model (ABAQUS, SIMULIA). The diaphragm geometry was partitioned into three different regions representing (i) clamping plate-diaphragm interface, (ii) connector-diaphragm interface and (iii) the gap between the two previous regions (see figure 19). The model was initially partitioned into four quadrilateral segments. Next to that it was laterally partitioned into two sections in order to achieve high mesh quality.

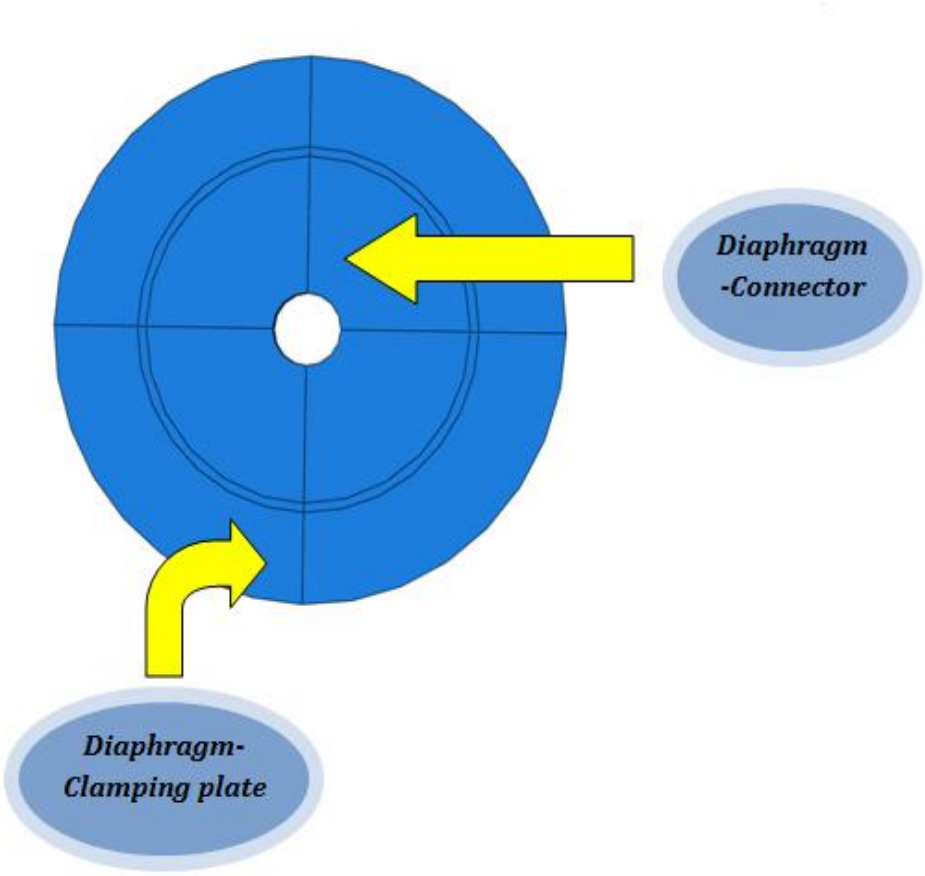

Figure 19: Partitioning strategy followed for the Finite element model of the diaphragm; the three contact regions are distinguished, while the quadratic partition is also highlighted.

The non-linear behavior of the silicon rubber material was captured by a Neo-Hookean hyperelastic material model with the following strain energy function:

$$W = C_1(I_1 - 3) + D_1(J - 1)^2 \ (1),$$

$$C_1 = \frac{\mu}{2} \ (2), where\ \mu\ is\ the\ shear\ modulus\ and$$

$$D_{1=}\frac{\kappa}{2} \ (3), where\ \kappa\ is\ the\ bulk\ modulus.$$

The material properties, assigned to the Neo-Hookean model were: $\mu = 0.36MPa$, $\kappa = 1500MPa$, ρ=1.1kg/m^3 and ν=0.49.

The step created for the analysis was Dynamic Implicit, which allows more accurate displacement-controlled simulations comparing to Dynamic explicit. NLgeom was turned on in order to account for the effect of large displacements. The Boundary Conditions were chosen to approximate the real contact of the diaphragm with the clamping plate and the connector. Therefore, the diaphragm-clamping plate interface was clamped by setting the option *ENCASTRE* on as shown in figure 20; that way all the displacement components were set equal to zero.

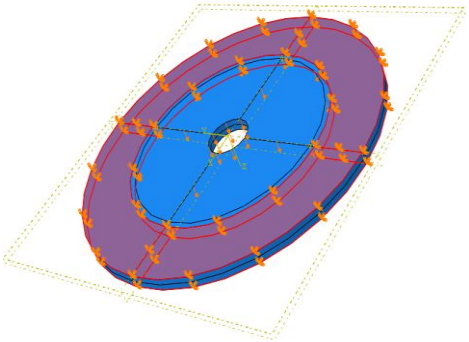

Figure 20: *ENCASTRE* boundary conditions for the diaphragm-clamping plate interface.

The segment defined by the connector-diaphragm interface, was considered to attribute to the total reaction force that is sensed by the load cell in the experimental setup. In ABAQUS, the reaction force is defined as RT and it is further characterized

by the components RT1, RT2, RT3 in x, y and z directions respectively. Due to the fact that the load cell is tension/compression, only the axial component RT3 was assumed to represent the force being detected by the load cell during real-time measurements. As illustrated in figure 21, a reference point and a kinematic constraint were set in order to obtain RT3 for the whole diaphragm-connector segment. A displacement/rotation boundary condition was prescribed to the reference point that allowed it to move at the same displacements as the ones applied in the experimental session. For each simulation, the applied displacement combined with the velocity of the indenter for the experimental session (0.15mm/sec) resulted in the estimation of the total step duration.

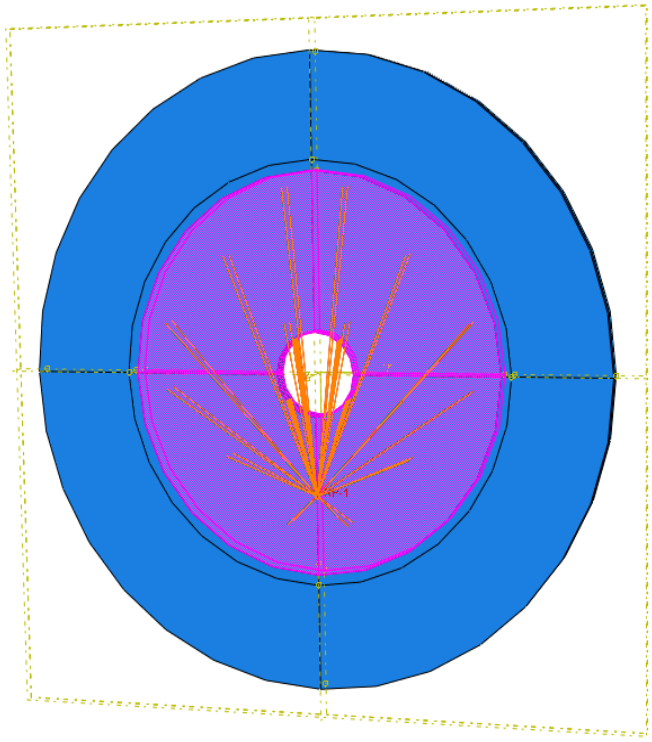

Figure 21: Kinematic constraints implemented in the model

The model was assigned with C3D8R reduced integration elements, while the number of elements was chosen based on a convergence study (see Appendix C). The model was finally assigned with 107712 elements, a number that constituted

the best compromise between accuracy and computational cost; the mesh that was generated is illustrated in figure 22.

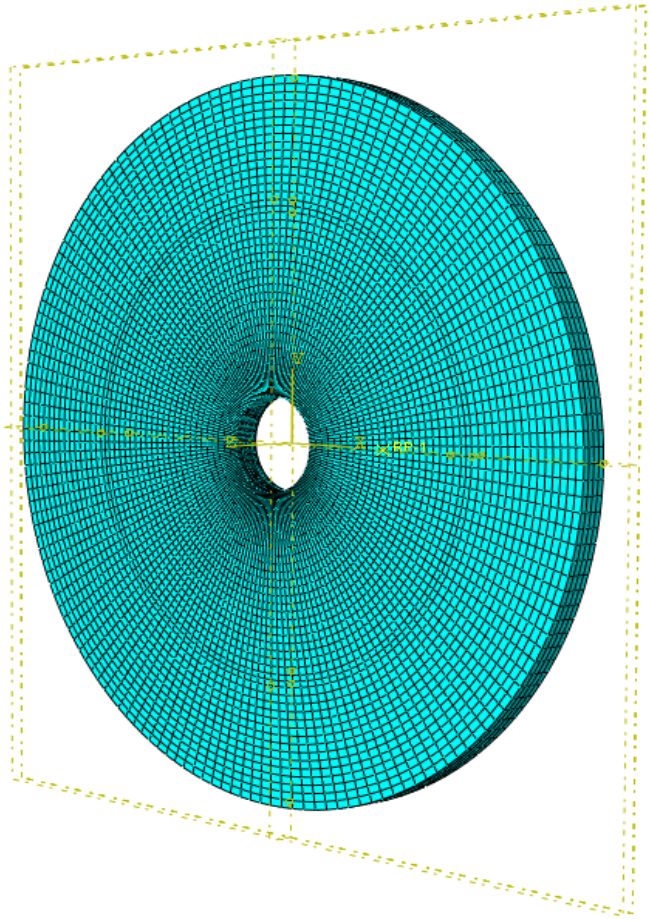

Figure 22: Finite Element Model Mesh consisting of 107712 C3D8R elements.

The comparison between the experimentally and computationally derived results is shown in figure 23.

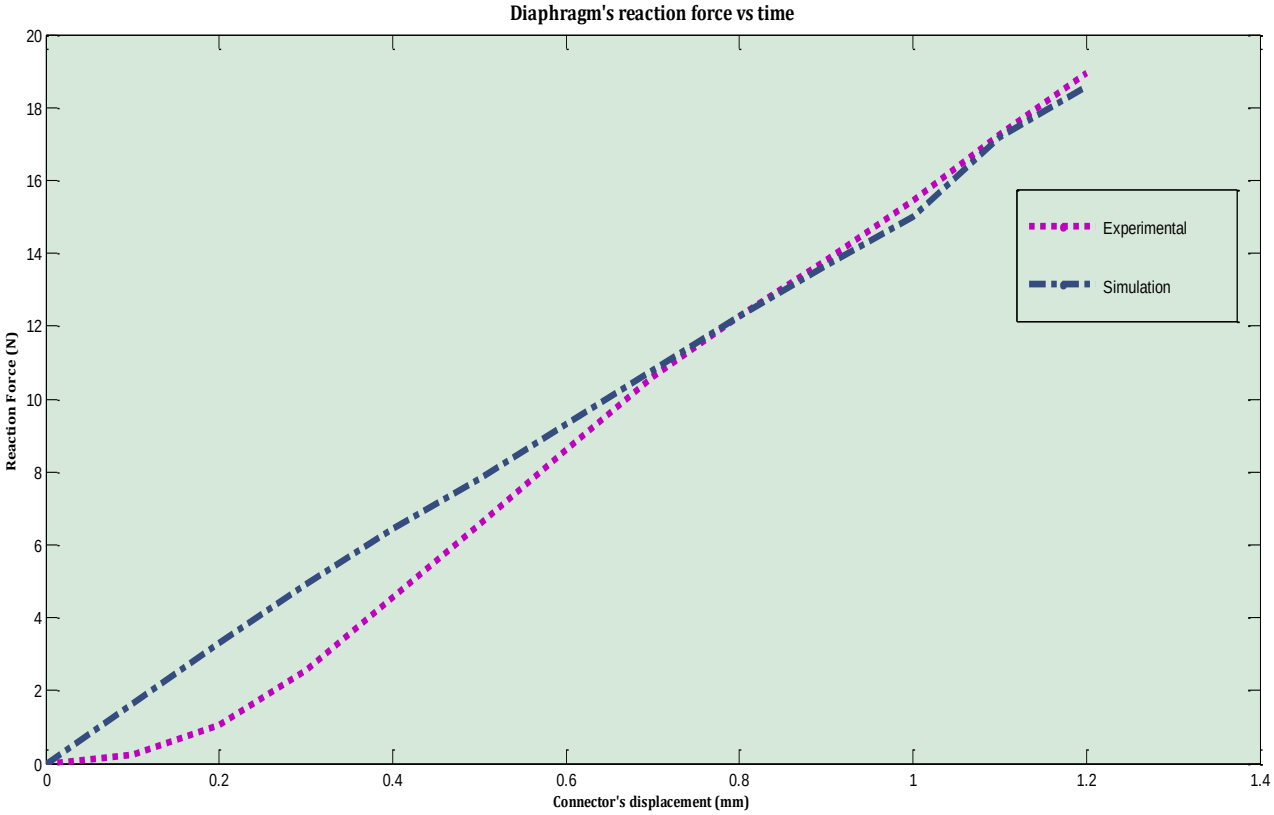

Figure 23: Comparison between the experimental and the computational results.

The real-time results indicated a non-linear material response up to a commanded displacement of 0.6mm, while a more linear trend was indicated for higher prescribed displacements. Additionally, after a commanded displacement of 1mm the reaction forces increased significantly. On the other hand in case of misalignment of the sample within the recess an adequate space between the sample and the indenter is required. That way any potential damage on the cartilage surface while assembling the various components of the device should be prevented. Thus, 1mm distance margin between the indenter and the sample was chosen. Accordingly, the indenter's length was set equal to 16mm, while the osteochondral plugs were attached on a POM substrate upon the wrapping procedure that ensured a total length of 15mm (see Design package for more detail); the assembled osteochondral plug is depicted in figure 24.

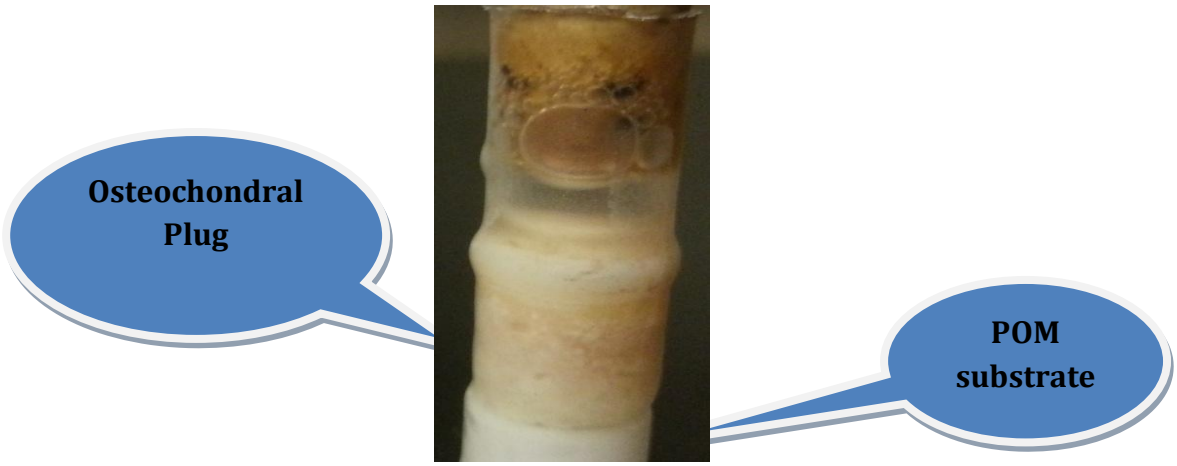

Figure 24: Representative Osteochondral plug with the associate POM substrate in order to achieve a total length of 15mm.

2.3 Measuring the mechanical properties

Apart from studying the dependency of solutes' transport on the loading conditions, the device can be additionally implemented for determining the mechanical properties of the cartilage with stress-relaxation tests. Particularly, the reaction force of the tissue upon specific displacement constitutes an indication of the sample's stiffness and it can further indicate mechanical properties, like Young's modulus and aggregate modulus. The validation of the device was performed with both soft and stiff samples in order to obtain an idea about the tissues that can be successfully measured. Therefore, cylindrical Ø8mm elastomeric samples were prepared in the Center of Mechanical Development of UMC in order to perform stress relaxation tests and monitor their reaction force. Additionally, soft cylindrical samples of the same diameter were punched from existing rubber sheets in the Precision and Microsystems Department of TU Delft.

The samples were subjected to 1mm displacement, which was applied with a velocity of 0.15mm/sec, and it was kept for a total time of 1 minute. For this part of the study a Ø12mm cylindrical indenter was used in order to apply the aforementioned unconfined stress relaxation pattern. We considered the starting point of the each test to overlap with the signal levels that correspond to the initial contact between the indenter and the

sample. Therefore when the load cell signal reached the approximate value of 0.2N we applied the loading pattern to the samples.

In total, 5 soft samples were subjected to the aforementioned stress relaxation profile; in this point it should be noted that for the stress-relaxation tests the device was oriented vertically. Additionally the membrane was omitted since the leakage-free operation of the device was not a prerequisite. The measurement accuracy of the device was evaluated by subjecting the previous samples under the same stress relaxation tests with the Zwick/Roell static test machine (1000N load cell). In order to create the same testing conditions as the ones that are encountered when using the Zwick device, the sample was not kept in place with the stabilizing screws. The reason is that the lateral clamping can potentially give rise to an additional force component that could create a significant discrepancy between the values measured by our device and the Zwick.

Preliminary stress relaxation tests in five samples indicated the sensitivity of the load cell to the external experimental conditions. This outcome indicated the need for performing the mechanical tests under smooth external conditions in order not to induce significant discrepancies in the results. Apart from external conditions, the effect of additional phenomena, like creep and dimensional stability of the plastic components were investigated and took into account upon the evaluation of the results (see Appendix D).

2.4 Control Unit

The mechanical loading device is controlled by a dedicated personal computer; the actuator is fully controllable and it makes the positioning feedback feasible by means of an integrated linear encoder (HAYDON KERK, Hybrid Stepper Actuator 17000 Series). The actuator comes with a custom made platform (IDEA KERK SOLUTIONS) through which the velocity, the displacement and the micro-stepping technique can be controlled. The fully controllable actuator allows to develop ramp profiles of various speeds and displacement regimes. The choice of the specific actuator was based on the space limitations that were described in previous chapter, as well as on the stroke length and the spatial resolution capabilities. At first glance, the spatial accuracy of the actuator constituted a significant parameter and for that reason a captive model was chosen. The spatial resolution, or in other words the distance per step was required to

be really fine; that way the setup allows the subjection of the cartilage to physiologically relevant loading conditions. Additionally, the stroke length was chosen to be big enough in order to ensure that the desired displacement for facilitating the contact of the indenter with the sample can be prescribed. At the same time, the stroke length is associated with the overall dimensions of the actuator, and therefore it shouldn't be significantly high due to the space limitation reasons explained before. Therefore, the stroke length was set equal to 50.8mm, while the resolution was chosen to be equal to 3μm. The smooth operation of the actuator under the command of infinitely small displacements was ensured via 1/64 micro-stepping technique.

A tension compression S-BEAM load cell (S-BEAM Junior Tension/Compression Load Cell, FUTEK FSH00104) was chosen in record the exerted forces. Furthermore, the load cell was chosen based on specific requirements in accordance with the literature records about the recorded forces for measuring the mechanical properties of cartilage. Typically, Bansal and his colleagues (Bansal et al., 2010) showed that depending on the stress relaxation pattern that will be applied the reaction force might exceed 25N. Thus, in order to provide the system with flexibility in load measurement, a 44.5N load cell was chosen (see figure 25).

Figure 25: Tension/Compression Load Cell for our device.

The electrical signals measured by the load cell are first amplified, converted into digital signals (National Instruments USB-6008 DAQ) and acquired by a custom-made LABVIEW platform (LABVIEW 2011 Student Edition, National Instruments). In order to obtain a stable signal, the amplifier was allowed to warm up for about 20 minutes. The particular combination of the DAQ card with the load cell ensured that the smallest detectable force that can be accurately predicted is 0.05N. By incorporating the load cell in the overall design the stiffness of the constructs can be monitored in the loading chamber during the time of the experiment. The load cell was calibrated with a 5-point calibration technique in TU DELFT MEETSHOP, in order to translate the voltage signals into force recordings, as shown in figure 25. Based on the calibration curve a custom LABVIEW data acquisition platform was developed and it is shown in figure 26.

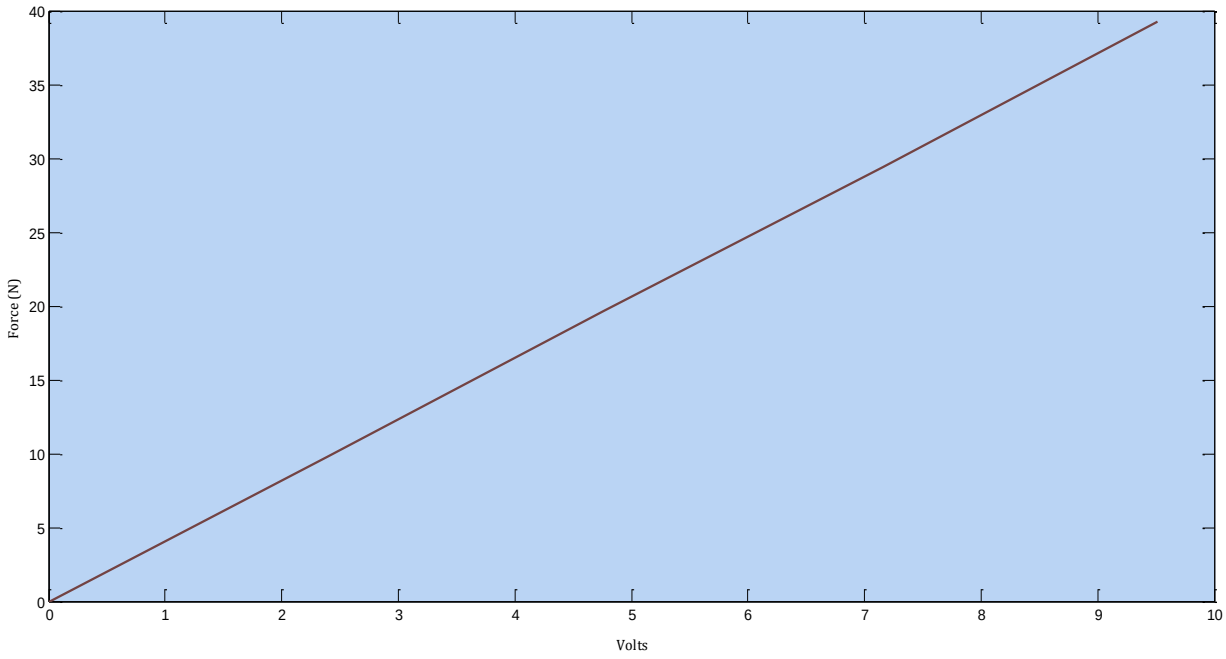

Figure 25: 5-point Calibration Curve of the S-BEAM Junior Tension/Compression Load Cell, FUTEK FSH00104).

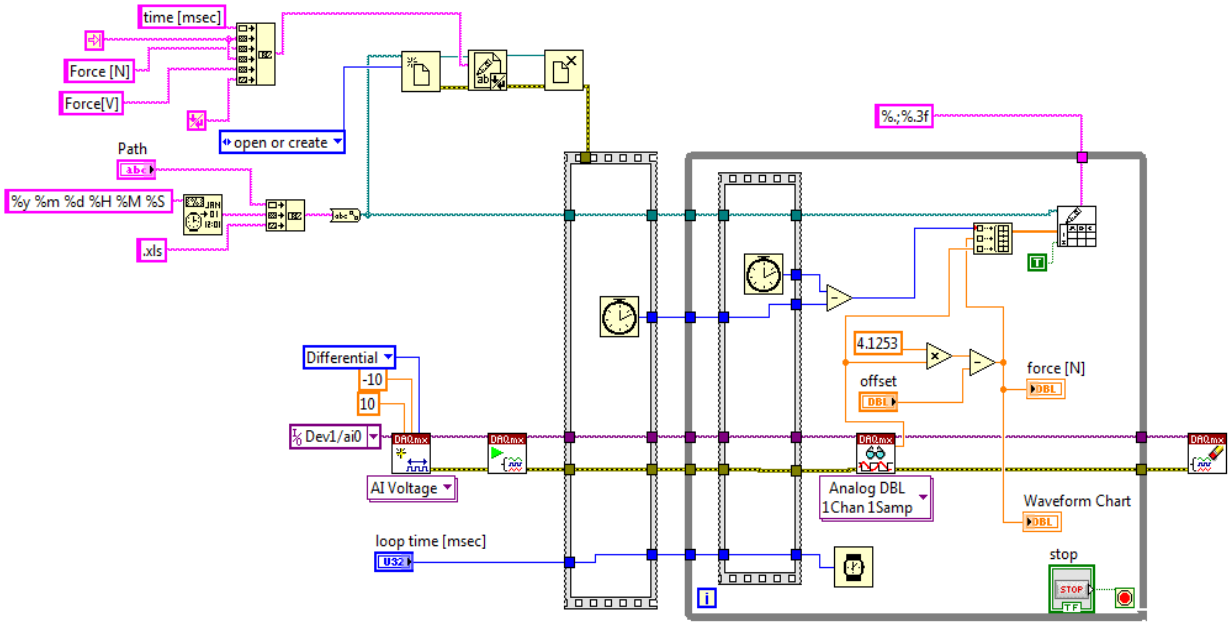

Figure 26: LABVIEW Platform for load cell data acquisition.

The CAD model of the assembled loading device is shown in figure 27; the real product is illustrated in figure 28 while a schematic representation of the device inside the micro-CT is given in figure 29.

The next step after designing and assembling the mechanical loading device was the design validation in order to ensure its suitability for the intended application. The validation steps followed in the context of this project are described in the next section, while a more concise analyze of the obtained results is given in the Discussion part.

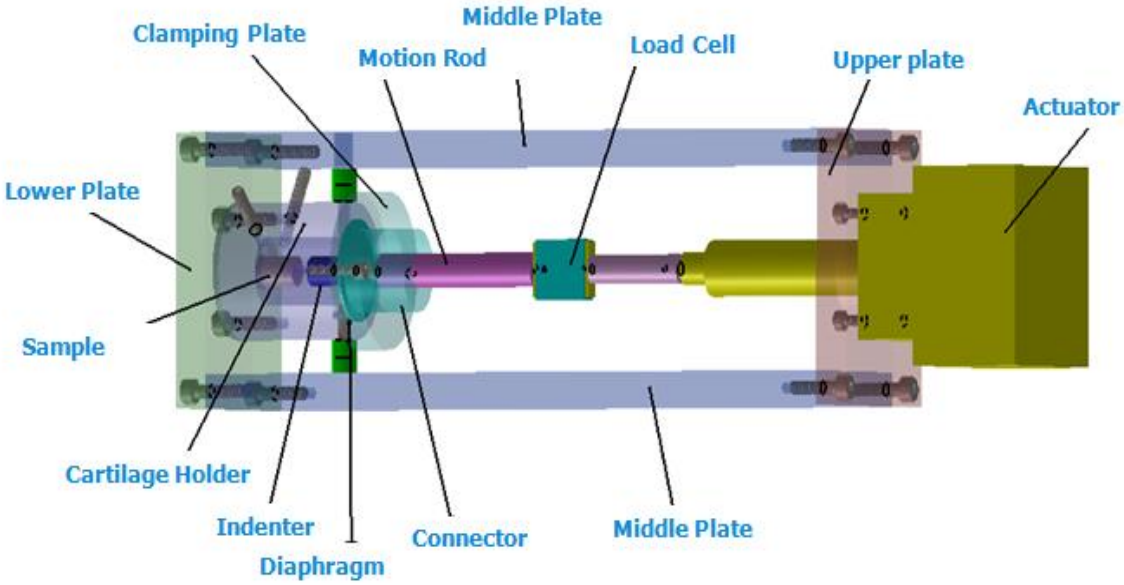

Figure 27: The CAD model of the assembled mechanical loading device.

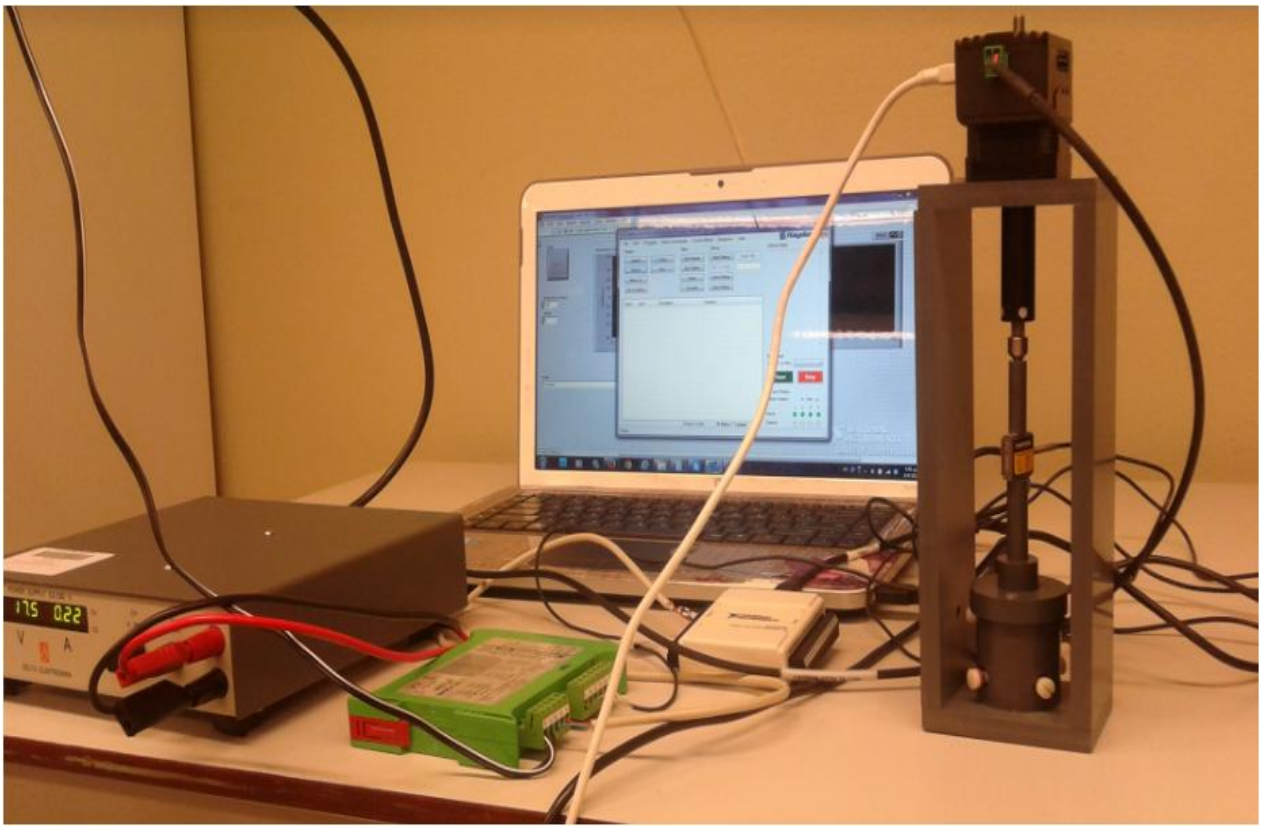

Figure 28: The mechanical loading device with the integrated control unit.

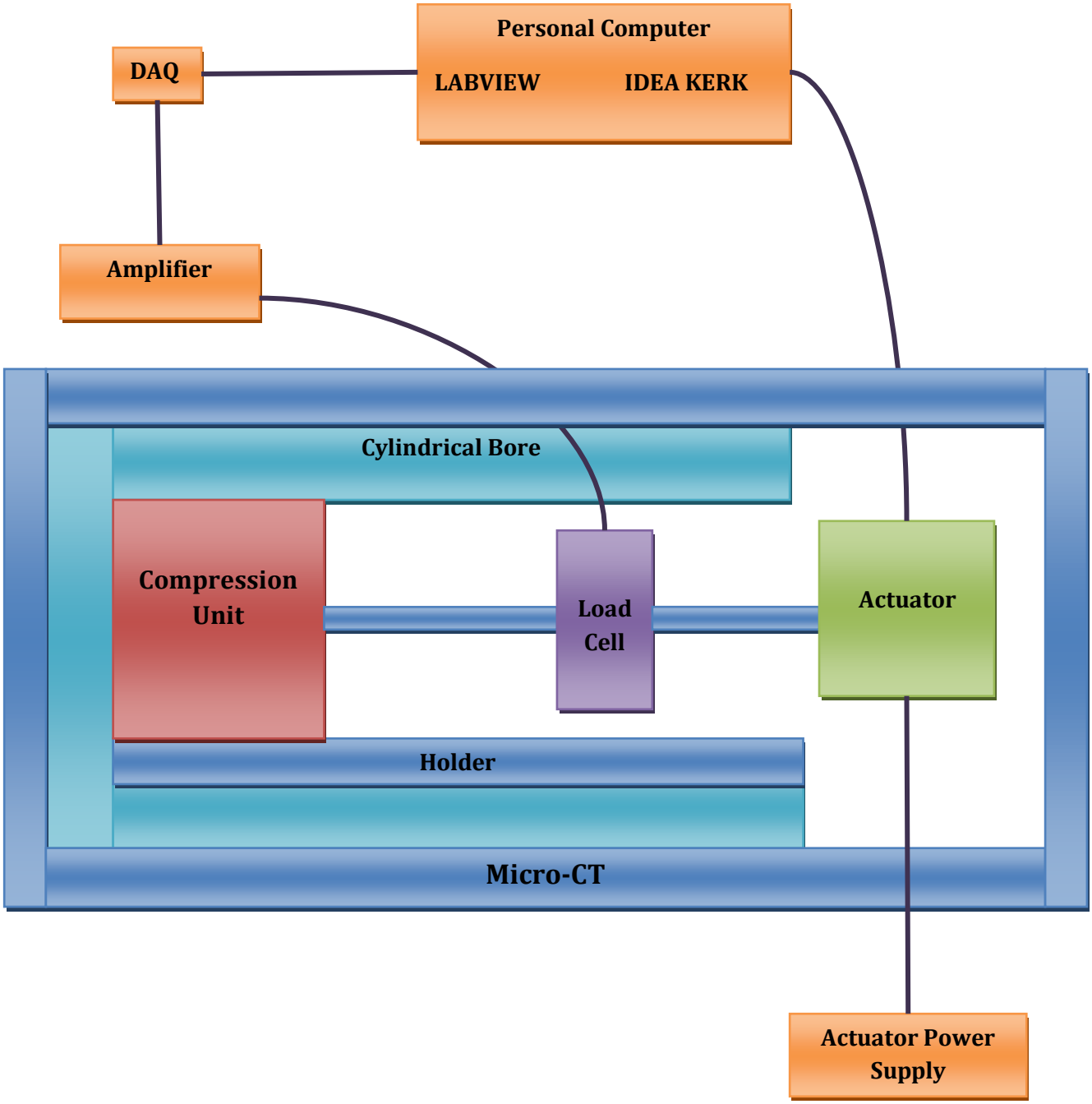

Figure 29: Schematic representation of the loading device in the micro-CT, together with the dedicated control system described before.

2.3. Validation

2.3.1. Leakage

First, we were required to ensure of leakage-free operation of the device in horizontal position. Therefore, the cartilage holder was filled with water and it was left horizontally positioned for 48 hours outside the micro-CT. During this time no leakage was observed either from the lateral side of the clamped diaphragm or from the sample clamping screws.

2.3.2. X-RAY hardening

Second, X-Ray scattering was checked after we filled out the holder with two different solutions of contrast agent. Using original concentration of contrast agent (Visipaque, 320mgI/mL) X-ray scattering could be observed. However by lowering contrast agent's concentration to half of its original value by means of dilution with distilled water (Visipaque, 160mgI/mL) the scattering effect remarkably decreased. Physiologic osmolarity of the solution (290mOsm) was maintained by adding required amount of sodium chloride. Consequently, we chose an appropriate solution for our experiments (Visipaque, 160mgI/mL, 290Mosm).

2.3.3. Concentric orientation of the system indenter-sample

The concentric orientation of the indenter with respect to the stabilized sample was evaluated through the micro-CT images (see figure 30).

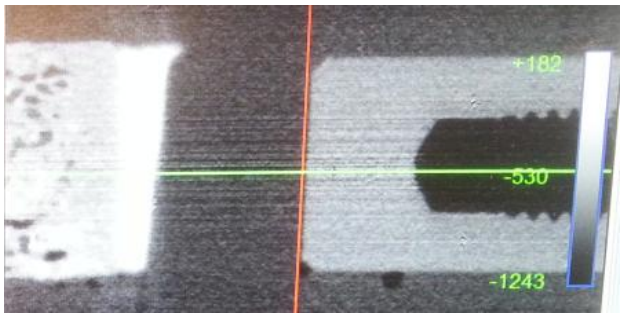

Figure 30: Concentric orientation of the indenter with respect to the sample.

2.3.4. Contact between the indenter and the sample

The signal change from the background levels measured by the load cell indicated the contact of the indenter with the sample. It is important to mention that the signal background levels measured by the load cell varied with respect to the device orientation, a fact that indicates the high sensitivity levels of the load cell. Therefore, for the vertical positioning of the device the initial force measured without any contact of the indenter with the sample corresponded to -0.08N. On the other hand, when the device was oriented horizontally the initial force before contact with the sample was equal to 0.08N.

The accuracy of the system in predicting the contact of the indenter with the sample was tested within the micro-CT. The cartilage holder was filled with water and the indenter was allowed to move towards the sample, while the option Live Mode was set in the system in order to observe the real time execution of the experiment. Upon change of the background level signal of the load cell to 0.17N, the micro-CT showed the contact of the indenter with the sample (see figure 31).

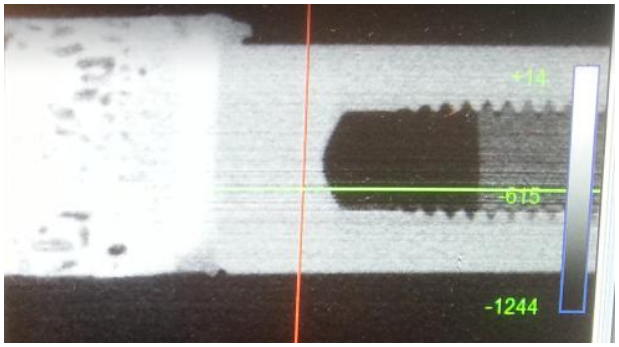

Figure 31: Contact of the indenter with the sample upon change of the background signal levels.

2.3.5. Measuring the mechanical properties

As describe before, we used soft elastomeric samples to compare stress-relaxation curves obtained by our device with stress-relaxation curves obtained from Zwick/Roell machine as the reference device. The results are shown in Figures 32-36.

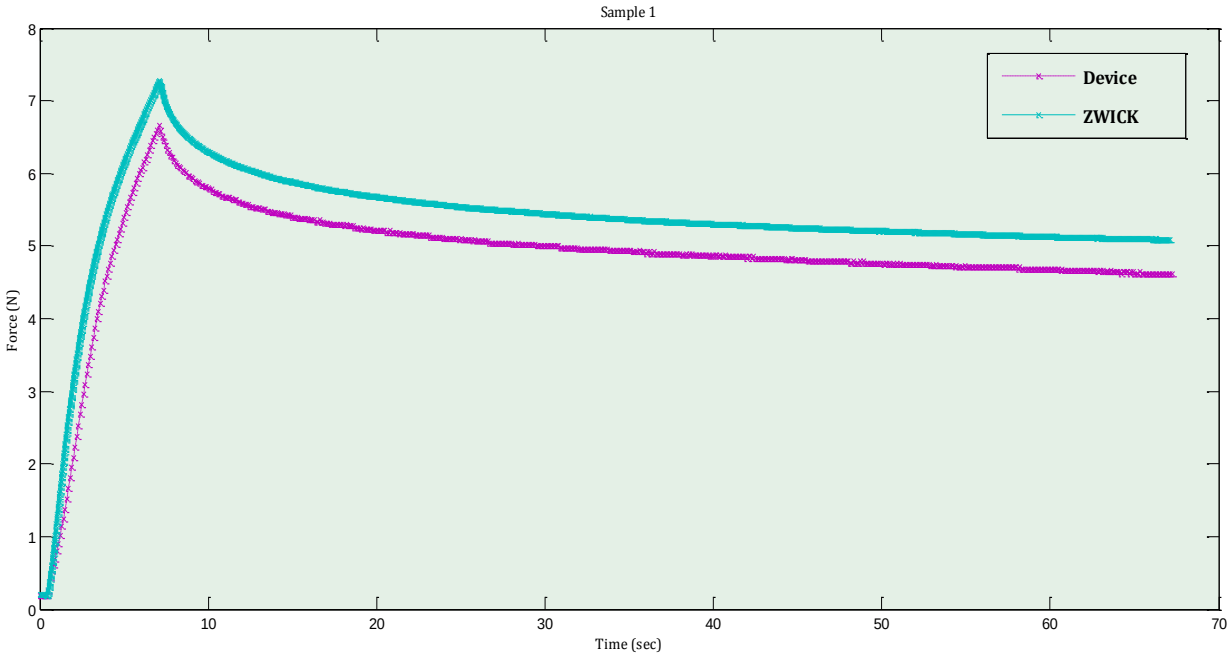

Figure 32: Stress-relaxation profile for the 1st soft elastomeric sample.

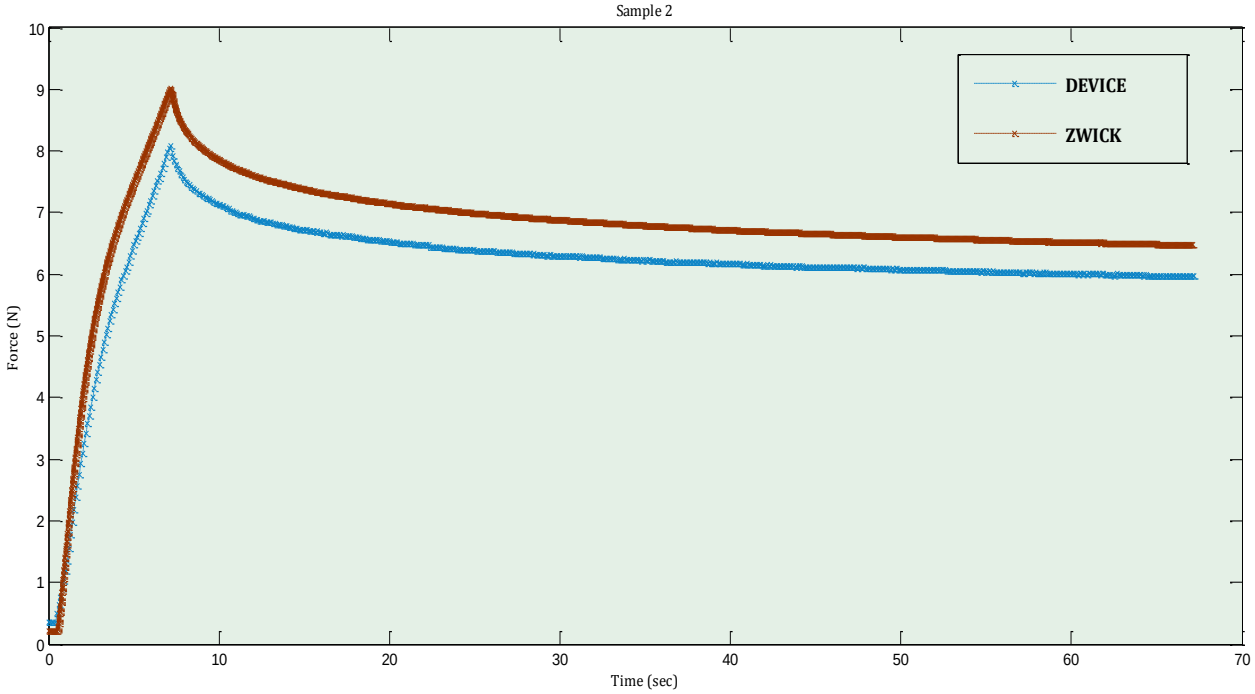

Figure 33: Stress-relaxation profile for the 2nd soft elastomeric sample.

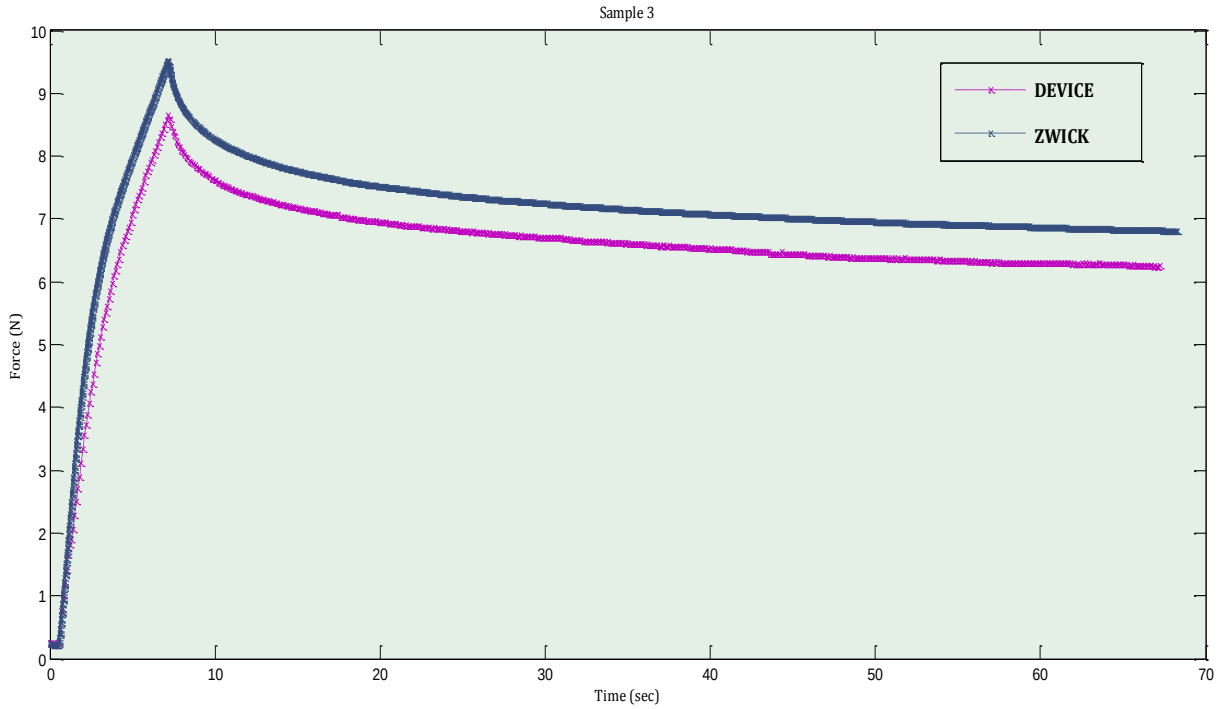

Figure 34: Stress-relaxation profile for the 3rd soft elastomeric sample.

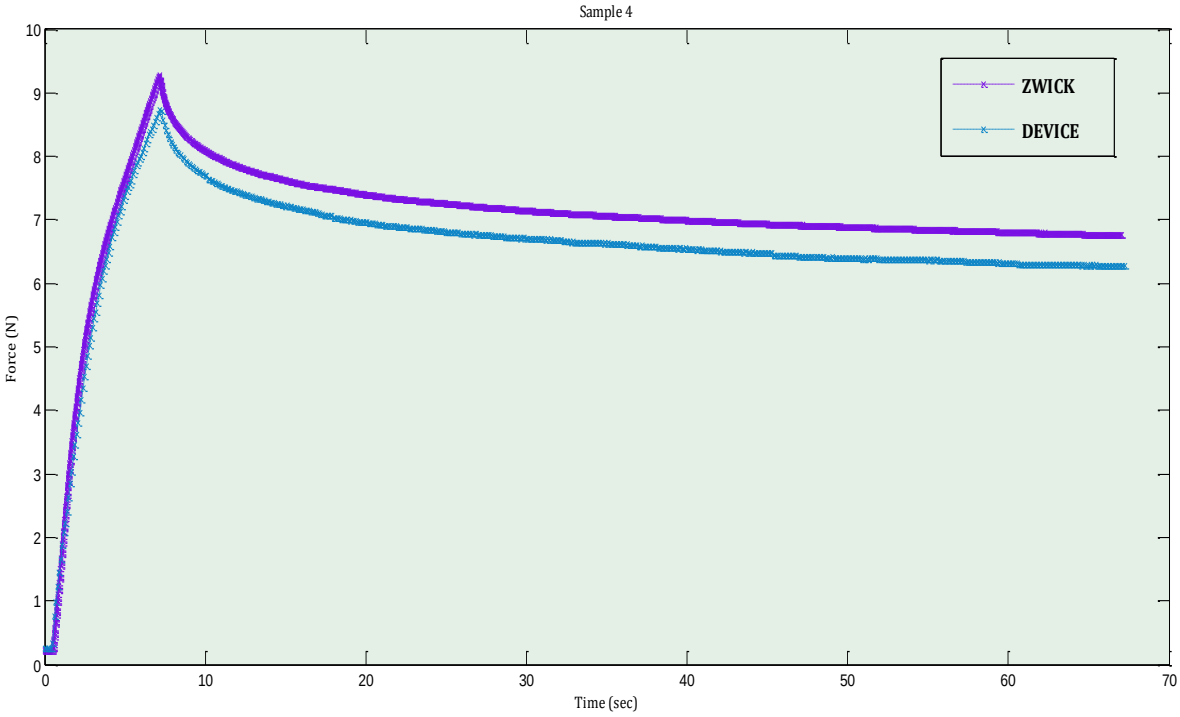

Figure 35: Stress-relaxation profile for the 4th soft elastomeric sample.

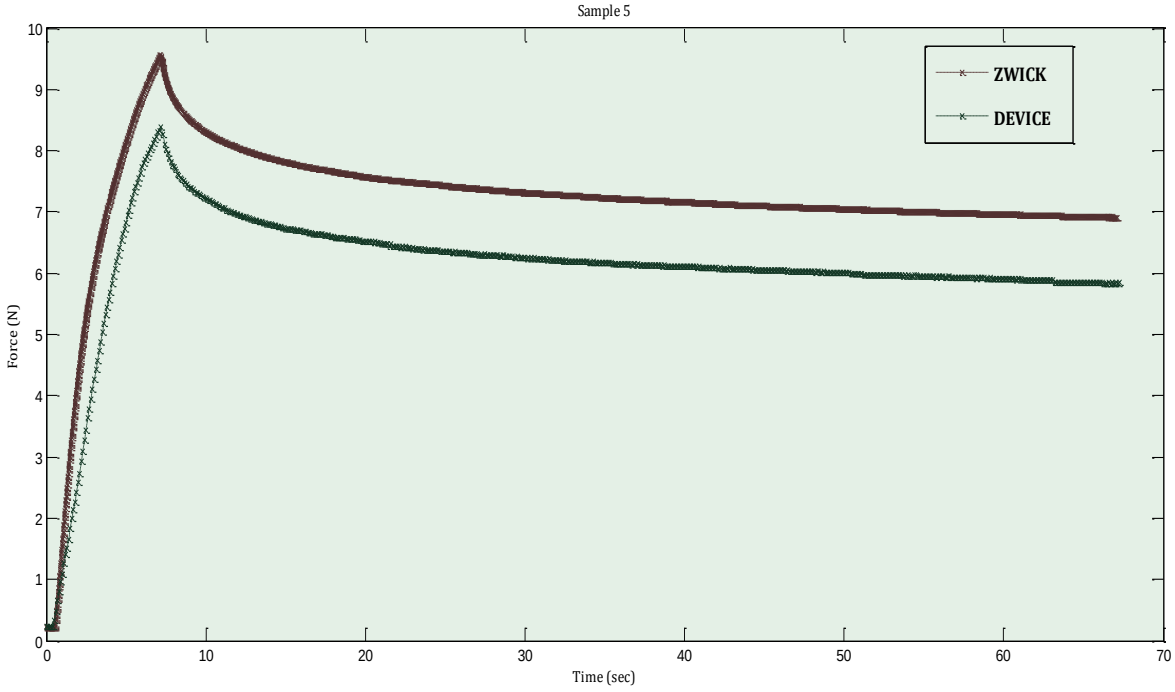

Figure 36: Stress-relaxation profile for the 5th sample.

The maximum reaction forces for each soft elastomeric sample as determined by our device and the Zwick/Roell device are shown in the table below; the average maximum force was estimated equal to 8.93N and 8.09N for the Zwick/Roell and the custom-made device, respectively (Standard deviations (STDs) are 10.67% and 10.92% respectively).

Table 2: Maximum reaction forces for the stress-relaxation patterns implemented as part of the device validation.

Sample	Maximum force ZWICK (N)	Maximum force our device (N)
1st	7.27	6.576
2nd	9.02	8.088
3rd	9.52	8.655
4th	9.27	8.74
5th	9.57	8.382

It should be noted that the measurement capabilities of our device didn't allow to capture mechanical properties of the hard elastomeric samples, as illustrated in figure 37.

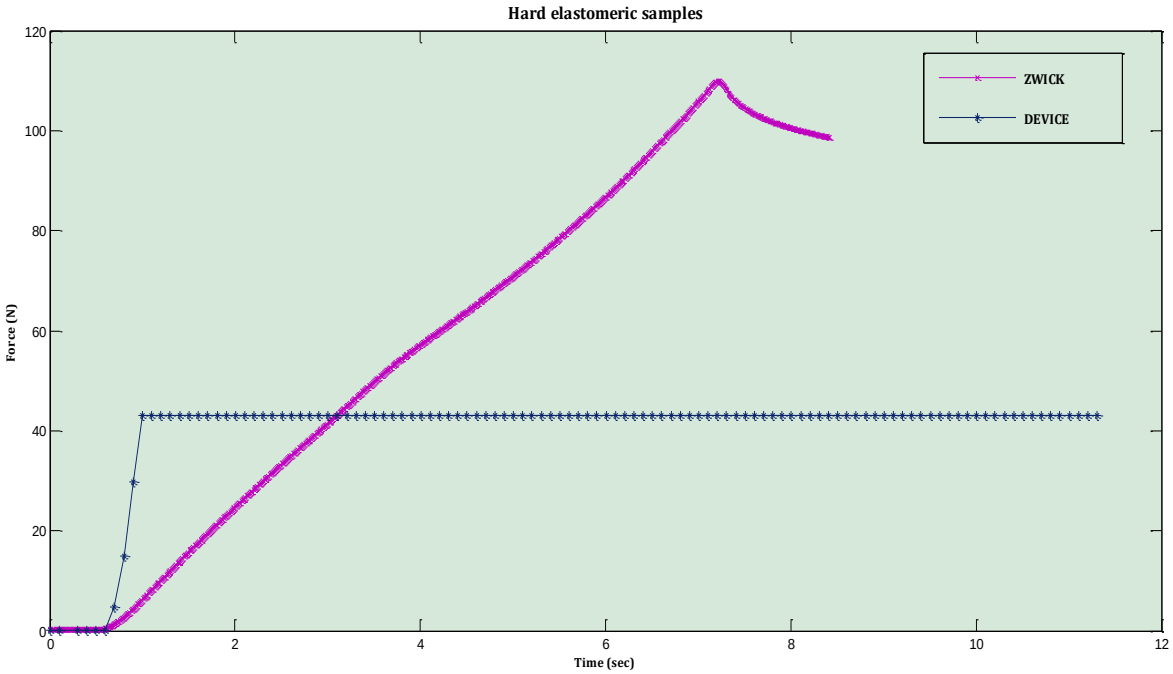

Figure 37: Stress relaxation test for the hard elastomeric sample.

3. Chapter II: Experimental procedure

3.1 Materials and methods

3.1.1 Experimental session

Equine osteochondral plugs were harvested and maintained in a mixture of PBS and protease inhibitors (Complete EDTA-free (ROCHE), 1 tablet/50ml solution, 5mM EDTA) in order to maintain the integrity of the tissue before wrapping procedure. As indicated before, the samples were wrapped with a special layer of heat-shrinking material in order to prevent lateral diffusion of contrast agent. The procedure consisted of positioning, where the sample was exposed to hot air for a few seconds while the surface of cartilage kept moist using a damp cotton plug. After the samples were wrapped a small amount of PBS with protease inhibitors was added on the top of the cartilage in order to prevent the degeneration of the tissue until the experimental

session. Next to that, an upper plug is placed on the top of the mixture in order to prevent evaporation. The schematic of the wrapped plug is illustrated in figure 38.

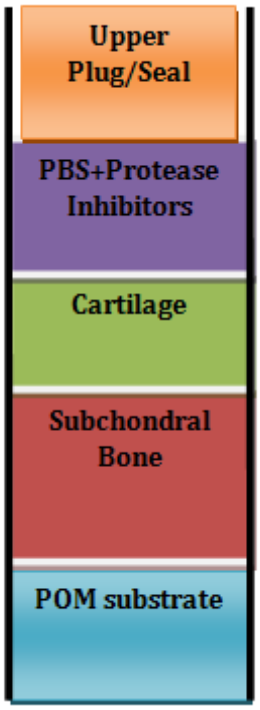

Figure 38: The wrapped osteochondral plug ready for the experiment.

The next step involved the proper positioning of the sample in the bottom recess of the cartilage holder. Thereafter, the stabilizing slotted screws penetrated until keeping the sample in place. Then Visipaque solution (*320mg/ml, 290mOsm, GE HEALTHCARE Netherlands*) was injected into the holder using the upper channel of the holder's reservoir. The Visipaque solution was injected into the reservoir space (approximately 8ml) until the reservoir containing the sample became full. In this point, it should be noted that for both static and dynamic experiments the mechanical loading device was used; for the case of the static conditions the indenter remained in its initial position, while for the loading conditions the indenter was commanded a displacement equal to 10% of the total cartilage thickness. The applied displacement was chosen based on the thickness of each sample. As shown in figure 39 the three samples were of non uniform geometry, while the average tissue thickness also varied from sample to sample.

Therefore, we estimated the average thickness value for each sample for various anatomical positions. The estimated values were 1.73mm, 2.63mm and 1.59mm for 1st, 2nd and 3rd sample respectively (the Standard deviations were 0.43, 0.33 and 0.15 for each sample respectively). After each static experiment (24 hours), the sample was immersed in a desorption bath consisting of PBS, inhibitor and EDTA for 48 hours at 5 ^{0}C to ensure the complete Visipaque wash-out.

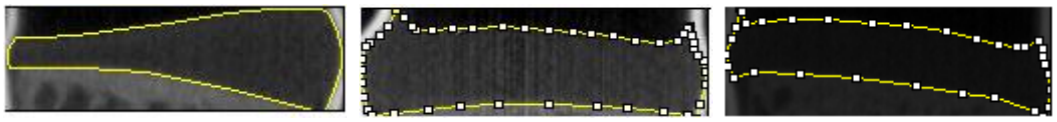

Figure 39 Micro-CT images showing the cartilage thickness of each sample. From left to right: Sample 1, Sample 2 and Sample 3.

After the whole setup was prepared, we placed the device into the micro-CT chamber (180 μA tube current, 90Kv tube voltage, 25^{0}C *QUANTUM FX PERKIN ELMER USA)* that is shown in figure 40; Live Mode was set on in order to ensure that the sample is properly positioned. The Field of View (FOV) was chosen equal to 30mm, which corresponds to a resolution of 60μm as described before. The scan technique was set equal to 3min in order to enhance image quality. Images were taken at discrete time points corresponding to 5min, 10min, 30 min, 1 hour, and respectively every one hour up to a total duration of 24 hours.

Figure 40: micro-CT used in our experiments.

3.2.2 Data Analysis

Data processing was performed with *ImageJ (1.47e)*, a public domain image processing software. The reconstructed images acquired from the micro-CT were first converted into .TIFF format *(Analyze 11.0)* and then the figure corresponding to the middle slice was imported to *ImageJ*. After being imported, the images were calibrated by assigning one maximum (100) and one minimum (0) grey value to the regions corresponding to contrast agent and air, respectively. The maximum and the minimum grey values were obtained through a stack's histogram. After the calibration process, a specific Region of Interest (ROI) consisting of the cartilage, a part of the contrast agent and part of the subchondral bone was created. Then, the chosen ROI was cropped and it was globally thresholded in order to isolate cartilage part from the contrast agent and the subchondral bone. The contour of the cartilage' mask was then placed on the calibrated image of the cartilage to obtain the average grey value. For better interpretation, the whole process is depicted in the flow chart below (see figure 41). The same process was repeated for all the time

points and the acquired grey values (representative of the contrast agent's diffusion were plotted against the time. The last step involved the subtraction of the initial grey value (t=0) from all the following values, in order to minimize the background noise and to obtain comparable results. The statistical significance of the results was evaluated by one-way ANOVA with 5% confidence level. For that reason only the final equilibrium grey value was taken for each sample under static and dynamic conditions, since it was assumed to be a good representation of the total contrast agent penetration across the cartilage.

Tiff Image

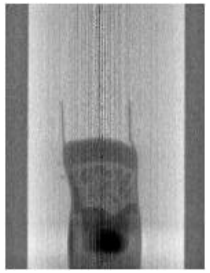

Histogram

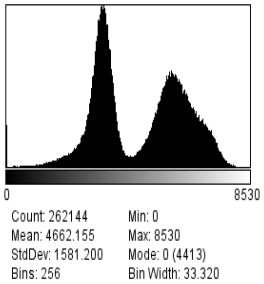

Calibration

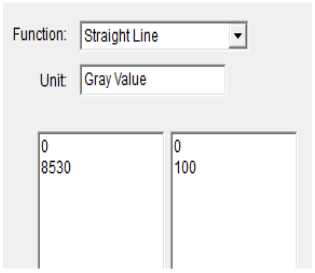

Initial ROI: Contrast agent+Cartilage+Bone

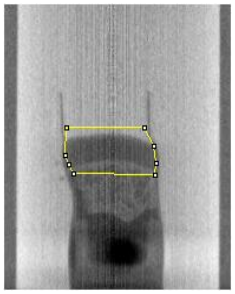

Cropped image with ROI

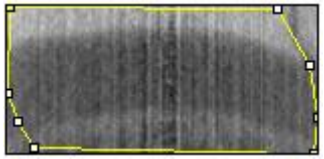

Threshold: Cartilage+Bone

Threshold: Cartilage+Contrast agent

Selected cartilage region

Copied region on the cropped image

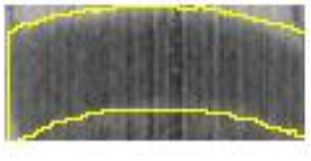

Analyze/ Measure

3.3.3 Results

The particular study aims at unraveling the effects of compression on Iodine solutes transport across equine articular cartilage. Therefore the grey values that represented the solutes' penetration were measured and they were plotted versus the discrete time points as described before. For each sample the grey values versus time were plotted under static and dynamic conditions, before and after subtraction respectively.

For sample 1the trend before subtraction of the initial value is illustrated in figure 42. The graph indicated that the equilibrium grey value of the static conditions was slightly higher than the corresponding value observed for the dynamic conditions. On the other hand, figure 43 illustrated a reverted trend after the subtraction step; particularly a 0.53% increase of the equilibrium grey value for the dynamic conditions was exhibited. Additionally, there was a remarkably steep increase of the contrast agent penetration at early time points as shown in both figure 42 and figure 43.

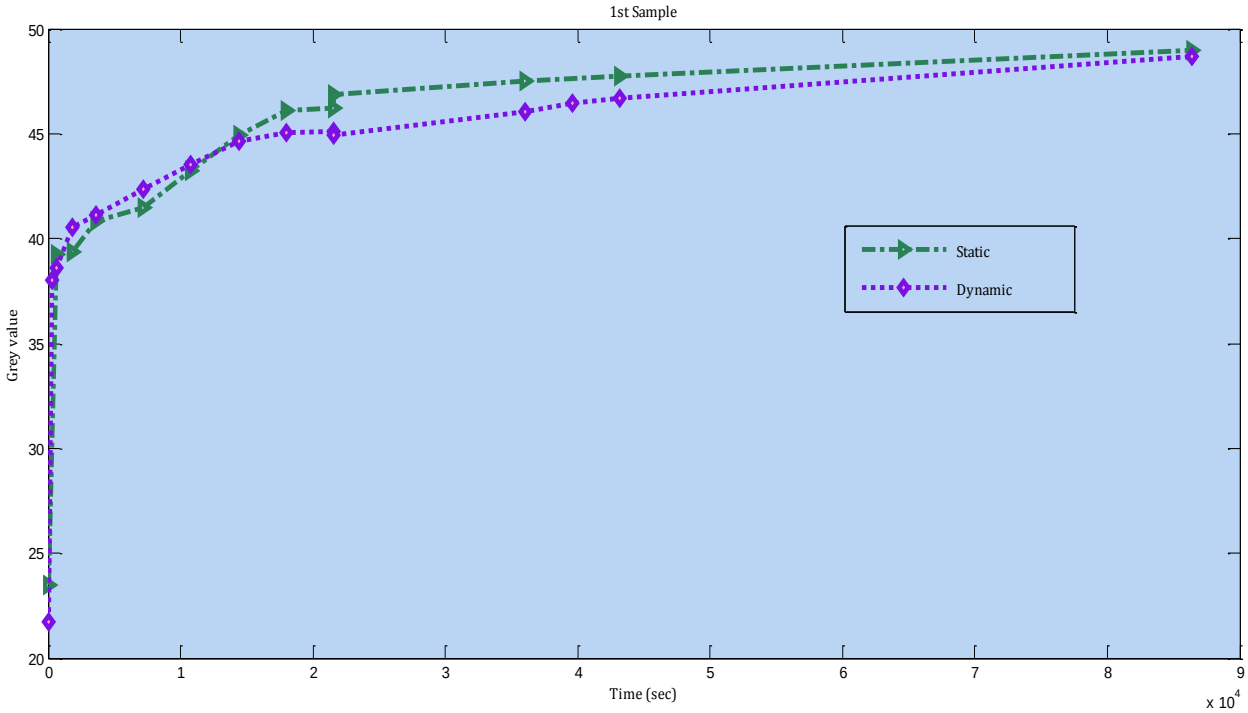

Figure: 42 Average Grey values vs. time for sample 1before subtraction.

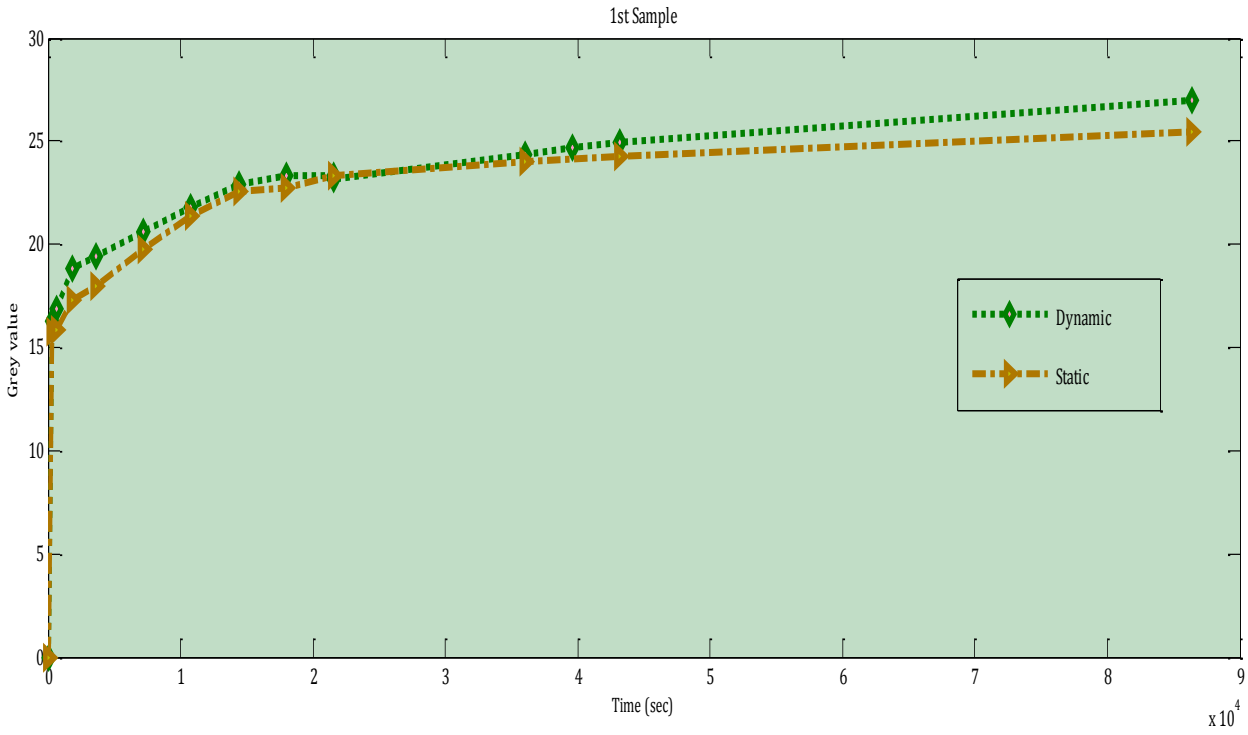

Figure 43: Average grey values vs. time for the sample 1 after subtraction.

Unlike sample 1, sample 2 exhibited a dramatic increase in average grey value at all time points under loading regimen. The trend was similar before and after subtraction of the initial grey value as illustrated in figure 44 and figure 45. An increase of 60.2% in contrast agent's penetration could be observed in sample 2 as a result of 10% compression.

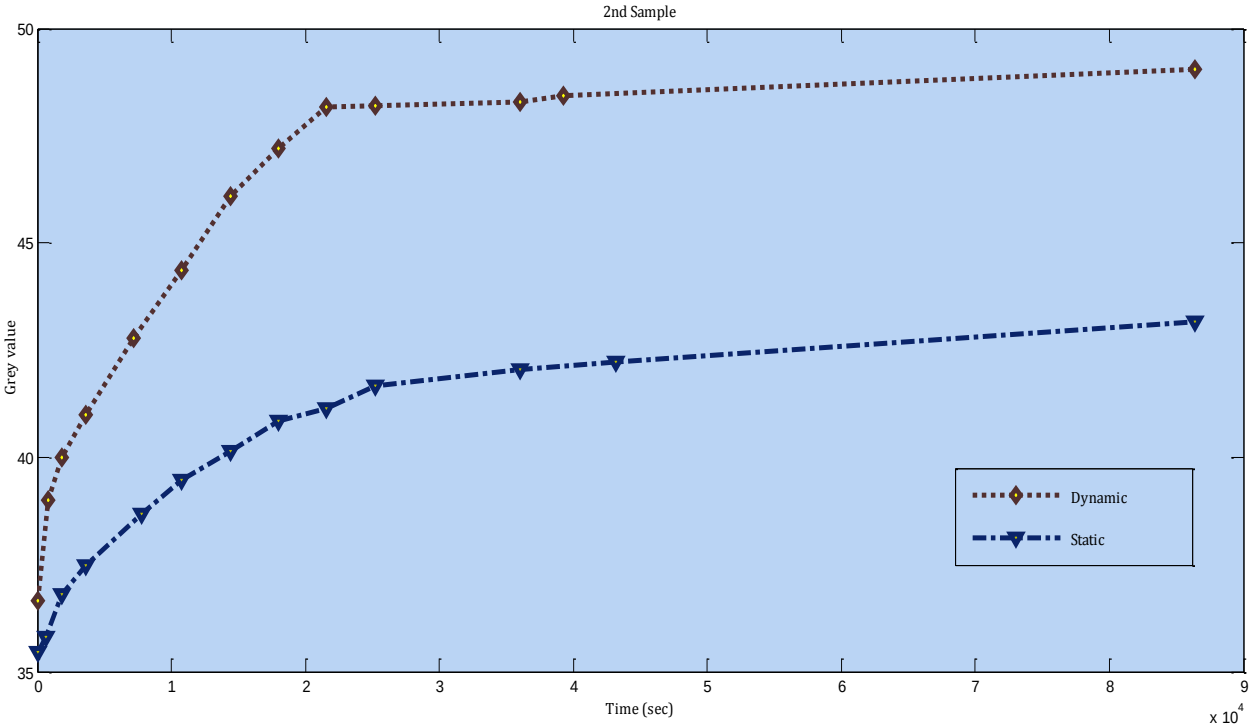

Figure 44: Average grey values vs. time for sample 2 before subtraction.

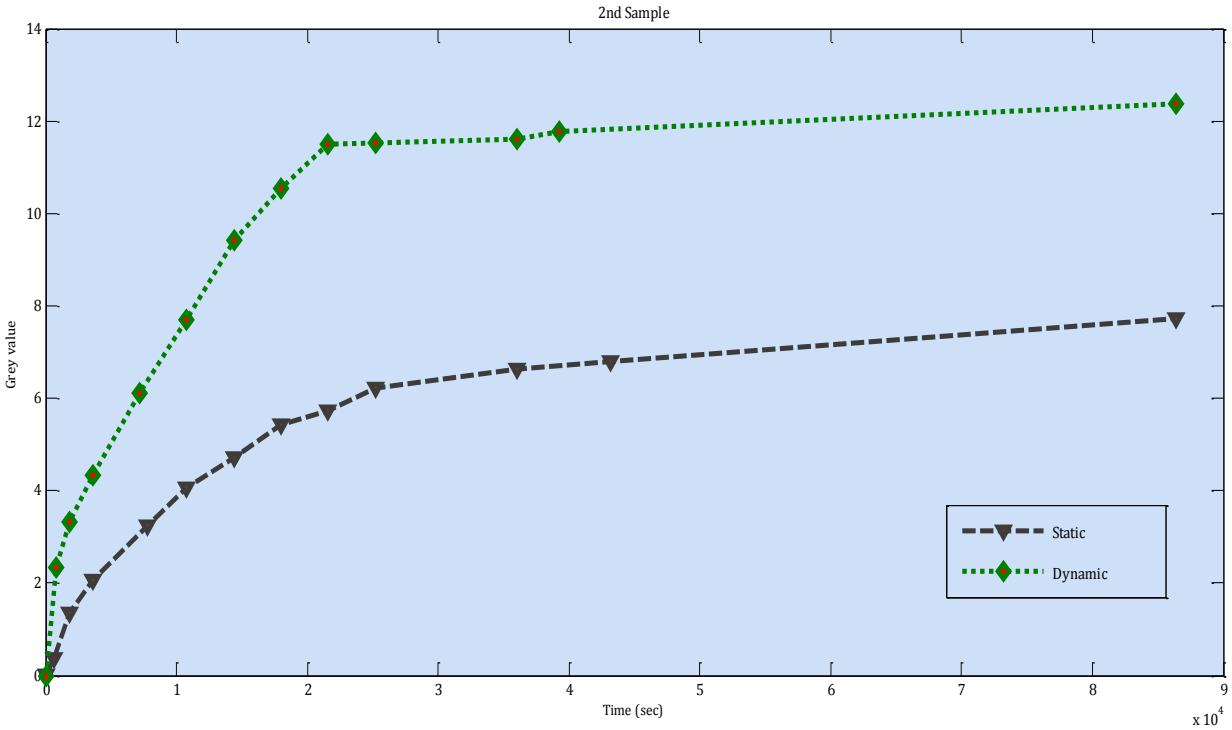

Figure 45: Average grey values vs. time for the sample 2 after subtraction.

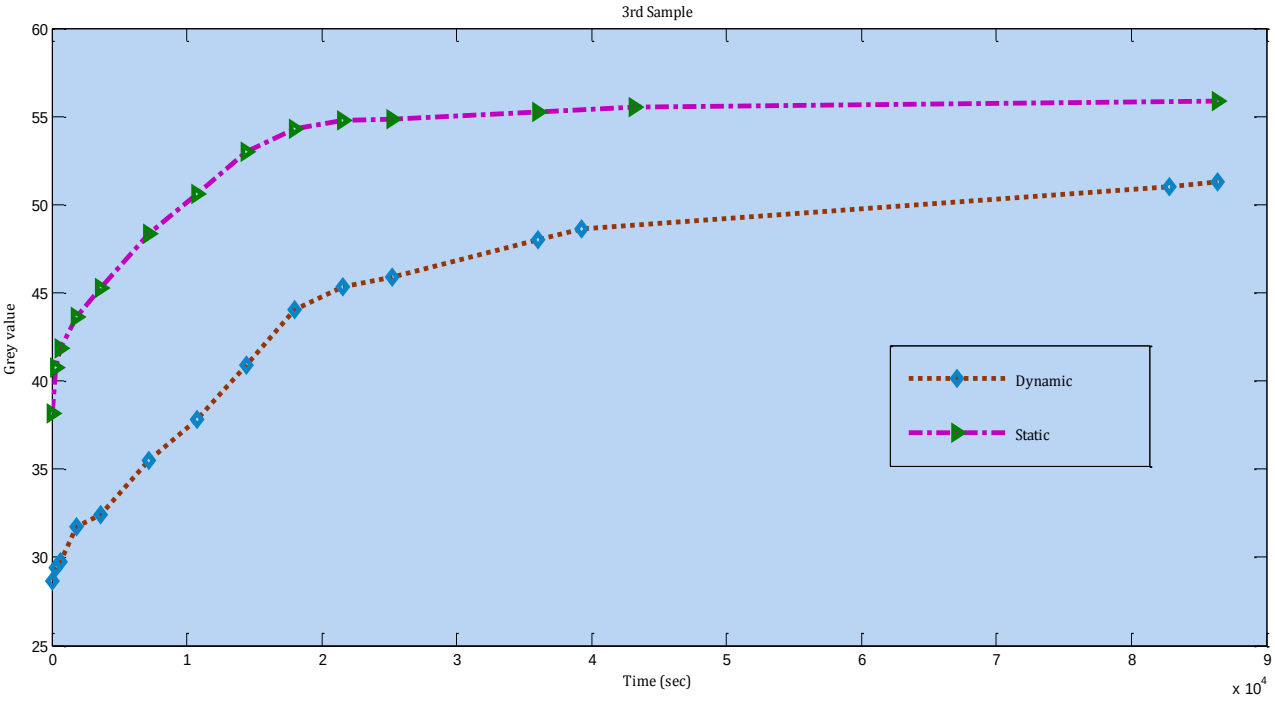

Graph 46: Average grey values vs. time for sample 3 before subtraction.

The trend that was obtained for sample 3 was different compared to those for sample 1 and sample 2. Regarding the grey values before the subtraction, they indicated a dramatic decrease of the contrast agent penetration under dynamic condition compared with the static condition. On the other hand, the subtraction step resulted in a profound grey value increase, but after the time point of 6 hours. Particularly, after 24 hours there was a 27.81% grey value increase compared with the equilibrium grey value for the static condition.

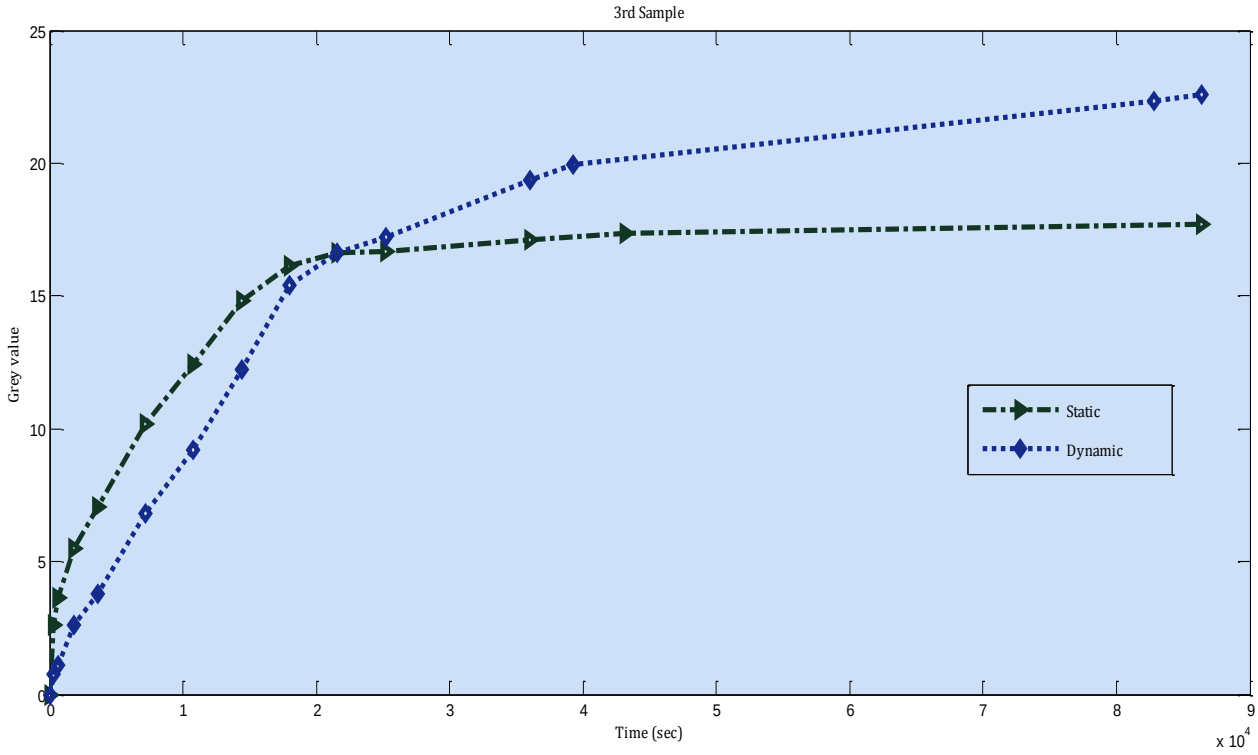

Figure 47: Average grey values vs. time for sample 3 after subtraction.

For the statistical analysis, the equilibrium grey value after subtraction was considered for both dynamic and static group as mentioned earlier. For better interpretation, the equilibrium grey value for each measurement is given in the table 3. The null hypothesis that was formed in order to implement ANOVA was the equality of the dynamic and the static average values. The statistical analysis followed showed that the increased contrast agent penetration at 24 hours under the dynamic conditions was not statistically significant.

Table 3 Equilibrium grey value for static and dynamic groups

	Static group	Dynamic group
Sample1	25.143	26.943
Sample2	12.377	12.377
Sample3	17.68	22.597
AVG	16.85	20.639
STD	36.23	51.86

4. Discussion

In this study, a novel device that allows cartilage diffusion studies under loading conditions in a micro-CT was developed. The clinically applicable CECT technique was implemented in order to investigate the effect of 10% compression ramp profiles on the transport of a neutral contrast agent (Visipaque). The penetration of the contrast agent from the lateral side was prevented, by wrapping the osteochondral plug with a layer of heat shrinking material; the reason why the study focused on the axial diffusion, is the associated increased clinical significance compared with the lateral diffusion. The device successfully operated in a micro-CT chamber with no evidence of X-ray scattering or contrast agent leakage. The successful performance of the device was primarily due to fabrication of the device components from rigid PVC as well as proper use of a silicon rubber diaphragm that literally separated the device intro two parts, allowing its leakage-free operation.

The diaphragm performance with respect to the exerted reaction forces under prescribed displacements of the connector was studied both experimentally and computationally. The diaphragm performance -with respect to the exerted reaction forces under prescribed displacements of the connector- was studied both experimentally and computationally. The diaphragm motion was simulated in *ABAQUS* as a Neo-Hookean hyperelastic model for nominal strain levels up to 1.2mm. In general a good correlation was observed between the computational and the experimental results, despite the fact that the initial non-linear response of the material could not be fully captured by the Neo-Hookean model.

Kim et al. who studied the stress response of chloroprene rubber versus prescribed strain values further confirms our results. Similar to the present work they investigated the response of chloroprene rubber both experimentally and computationally using a Neo-Hookean, Mooney-Rivlin and Ogden hyperelastic material models. Despite the fact that up to a nominal strain equal to 1, the Neo-Hookean model was in good correlation with the experimental data, again the initial non-linear response could not be observed (Kim et al., 2012). However, for the purpose of the particular study the Neo-Hookean model allowed accurate prediction of the reaction forces for high strain levels.

Therefore, the model was proved accurate enough for the particular purpose. Thus, we combined the computational results with the experimental results in order to select the right indenter length for our study.

The accuracy of the device was validated through stress relaxation tests on both hard and soft elastomeric samples, which were performed in our custom-made device and in a *Zwick/Roell* instrument located in the Precisions and Microsystems Department at TU Delft. Soft elastomeric samples (n=5) were subjected to a stress-relaxation profile that was in alignment with the loading pattern implemented for the convection study. The average maximum force recorded from the custom-made device was 9.42% lower compared to the corresponding maximum force from the ZWICK instrument. The observed discrepancy is most likely attributed to the different nature of the two experimental setups. The custom-made device was made of rigid PVC, a material that is stiff enough among other plastic materials but is not comparable with the metallic materials from which the *Zwick* instrument was made. Additionally, the small-level dimensional instability of the compression unit resulted in a decrease of the applied displacement and therefore resulted in a reduced reaction force compared to the *Zwick* instrument (see Appendix D). On the other hand, the custom-made device was proved insufficient to allow the measurement of stiffer samples. Besides limited loading capacity of the load cell, the relatively fragile nature of the setup compared with the *Zwick* instrument contributed to an inaccurate stress-relaxation response. Thus, it has become obvious that the device could be appropriately used to measure the properties of relatively soft samples.

The fine resolution of the micro-CT enabled high imaging quality and therefore enhanced the value of the present study. Additionally, the dilution of VISIPAQUE with water minimized potential scattering effects, while it maintained the physiological osmolarity conditions of the cartilage. Therefore the results were independent from physicochemical alterations of the tissue, which could affect the penetration pattern of the contrast agent. One osteochondral plug per time underwent physiologically relevant compression regimens for convection studies. The preliminary results presented in this study indicated beneficial influence of the applied loading regimen on the penetration of neutral iodine solutes across articular cartilage. Typically, the comparison between the results obtained for sample 2, indicated an approximately 3-fold increase of the contrast agent equilibrium under loading conditions, comparing to the static conditions. The

increase is potentially attributed to the high compression velocity (0.15mm/sec), which induced high fluid flow and therefore enhanced the transport procedure. It should be further noted that compression also makes the cartilage become more compact that might hinder the penetration of bath's molecules. The increased equilibrium grey value in loading condition can explain that induced fluid flow plays a more important role than compactness of the cartilage itself. It can also be inferred from the corresponding curves for samples 1-3 that major enhancement in the transport rate in loading condition especially at early time points sheds light on the essential role of modulated fluid flow within cartilage's matrix. Next to that, the nature of the porous indenter allowed for continuous transport of the solutes across the tissue surface upon loading regimen. Therefore, there is a proof that the specific pattern enhances the penetration of the solutes, and it can be therefore implemented when the issue of effective nutrients transport is under investigation.

A profound increase was also noticed for the sample 3 but with a different pattern this time; particularly, the grey value increased after the time point of 6 hours, while before that the observed increase was in favor of the static conditions. Another parameter that possibly affected the transport phenomena under the dynamic conditions was the variations among the contact patterns that were observed each time between the indenter and the sample. As stated in previous section, the concentric orientation of the sample with respect to the indenter was approached as much as possible. However, the geometry of the cartilage holder bottom recess together with the preload applied by the stabilizing screws affected the concentric positioning of the sample. Those variations accounted for the different contact patterns that were observed upon the application of the compression regimen, and are shown in figure 48. Among the three different sessions, full contact was achieved for the sample 3 only. Therefore, it can be concluded that the observed statistical insignificance was correlated to the geometrical differences in the cartilage samples i.e. thickness as well as to the slightly different contact between the indenter and the cartilage's surface. However, considering the equilibrium average grey value as a criterion for increased transport might not be fully appropriate. Therefore, investigations regarding diffusion rate in various time points might provide even a better explanation for the effect of compression on the facilitation of the transport. Additionally, the plastic nature of the setup is very likely to have affected the

loading conditions, in a manner similar to the one observed during the measurement of the mechanical properties of soft elastomeric samples.

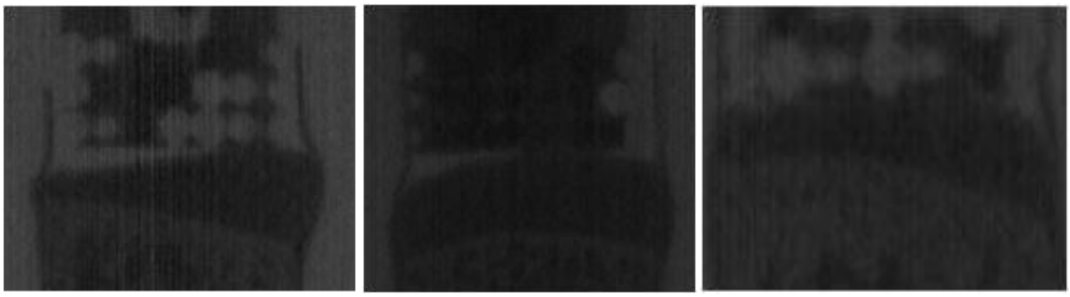

Figure 48: Micro-CT images revealing the different contact patterns; from left to right: Contact pattern indenter-sample for the 1st, 2nd and 3rd sample.

The particular project aimed at evaluating the effect of a specific loading regimen on the mechanism that derived the transport of Iodine solutes across articular cartilage. Apart from the novel setup that involved the horizontal orientation of the mechanical loading device inside the micro-CT, also the specific loading pattern has been rarely implemented. Particularly, the strain rates that have been most commonly implemented do not exceed $8x10^{-3}$mm/sec in order to assume quasistatic conditions (Evans and Quinn, 2006, Popp et al., 2012)**.** In our project we chose to dramatically increase the compression velocity in order to induce high fluid flow within the matrix. Therefore, the need for further investigation of the effects of the particular loading pattern on tissue integrity and subsequently on the transport mechanism rises. For that purpose higher sample size is required, while the samples should be carefully drilled in order to ensure that their thickness is as uniform as possible.

Additionally, the value of the study can be further increased by estimating the diffusion coefficient, as well as the convection which indicates the penetration rate of the solutes. Particularly for ramp profiles, it has been shown that while the solutes penetration and the convection coefficient, the diffusion coefficient might be adversely affected (Quinn et al., 2001). Moreover, the time frame that we chose to apply 10% ramp compression was in contradiction with the time pattern followed by Quinn and his

colleagues in the sense that the later was implemented step-wise. Therefore it becomes obvious that more research is essential in order to form a concrete outcome from our study.

Nevertheless, the present design constitutes a novel approach towards the study of transport phenomena across cartilage applying CECT method. Brainstorming and verification process were performed based on three basic criteria: leakage-free operation, no adverse scattering phenomena and micro-CT space limitation. Those requirements were optimally met by plastic material choice, a diaphragm-based motion unit and horizontal orientation of the device inside the micro-CT. The mechanical loading device was validated upon service, where no adverse phenomenon, like leakage took place. On the other hand the plastic components induce an inaccuracy factor on the desired levels of applied displacement (see Appendix D); the same is applicable for the measurement of the mechanical properties when needed. The particular condition could be possibly eliminated by reducing the overall length of the components that consisted the integrated motion unit (see Appendix D).

To conclude, the present device constitutes a clinically applicable tool, since it gives insight in crucial topics like the optimal transport conditions under which the cartilage's biological response is favorably affected. Despite being statistical insignificant, an increased solutes penetration under dynamic conditions was shown compared to non loading conditions. From the clinical point of view, the optimal transport parameters may contribute to the construction of viable tissue engineered constructs towards the treatment of severe conditions like OA. Next to that, studying the effect of loading on solutes transport within a micro-CT might be a useful guide for the physicians, in the sense that it allows them to determine the motion patterns that would increase the diffusion of contrast agents within patients' cartilage during CECT imaging. Additionally the device allows the estimation of the tissue integrity by determining its material properties with properly established unconfined stress relaxation tests. Next to that, it can be implemented in order to diagnose osteoarthritic sample, while it can constitute a tool that determines the loading patterns that favorably or negatively affect the progression of Osteoarthritis. Particularly, the non-Fickean phenomena can be additionally introduced to the existing experimental setup and the disease severity can be determined through the penetration rates of negatively charged solutes.

Acknowledgements

I would like to thank all those who actively contributed to the realization of my thesis. Thanks to the DEMO Mechanical Development team, for the conversations, the valuable advice on technical aspects and finally the manufacturing of the mechanical loading device. Thanks to Jos Van Driel from 3ME Meetshop the nice journeys in the electronics' world. Thanks to the Precision and Microsystems Team in 3ME for allowing me to use the ZWICK instrument and therefore come to a robust conclusion for the capabilities of my device.

Finally, I am grateful to have next to me people like my family and my good friends who constantly supported me and allowed me to share with them concerns and worries that were sometimes present during this year. Thanks for being patient with me, without complaining that I was sometimes overdoing it (indeed!); without you this project wouldn't have been complete.

References

ARMSTRONG, C. G., BAHRANI, A. S. & GARDNER, D. L. 1979. In vitro measurement of articular cartilage deformations in the intact human hip joint under load. *Journal of Bone and Joint Surgery - Series A,* 61**,** 744-755.

ATESHIAN, G. A., MAAS, S. & WEISS, J. A. 2012. Solute transport across a contact interface in deformable porous media. *Journal of Biomechanics,* 45**,** 1023-1027.

ATESHIAN, G. A., WARDEN, W. H., KIM, J. J., GRELSAMER, R. P. & MOW, V. C. 1997. Finite deformation biphasic material properties of bovine articular cartilage from confined compression experiments. *Journal of Biomechanics,* 30**,** 1157-1164.

ATHANASIOU, K. A., ROSENWASSER, M. P., BUCKWALTER, J. A., MALININ, T. I. & MOW, V. C. 1991. Interspecies comparisons of in situ intrinsic mechanical properties of distal femoral cartilage. *Journal of Orthopaedic Research,* 9**,** 330-340.

AULA, A. S., JURVELIN, J. S. & TÖYRÄS, J. 2009. Simultaneous computed tomography of articular cartilage and subchondral bone. *Osteoarthritis and Cartilage,* 17**,** 1583-1588.

BANSAL, P. N., JOSHI, N. S., ENTEZARI, V., GRINSTAFF, M. W. & SNYDER, B. D. 2010. Contrast Enhanced Computed Tomography can predict the glycosaminoglycan content and biomechanical properties of articular cartilage. *Osteoarthritis and Cartilage,* 18**,** 184-191.

BOSCHETTI, F., PENNATI, G., GERVASO, F., PERETTI, G. M. & DUBINI, G. 2004. Biomechanical properties of human articular cartilage under compressive loads. *Biorheology,* 41**,** 159-166.

DAVISSON, T., KUNIG, S., CHEN, A., SAH, R. & RATCLIFFE, A. 2002. Static and dynamic compression modulate matrix metabolism in tissue engineered cartilage. *Journal of Orthopaedic Research,* 20**,** 842-848.

DÉMARTEAU, O., WENDT, D., BRACCINI, A., JAKOB, M., SCHÄFER, D., HEBERER, M. & MARTIN, I. 2003. Dynamic compression of cartilage constructs engineered from expanded human articular chondrocytes. *Biochemical and Biophysical Research Communications,* 310**,** 580-588.

EVANS, R. C. & QUINN, T. M. 2006. Solute convection in dynamically compressed cartilage. *Journal of Biomechanics,* 39**,** 1048-1055.

GRAD, S., GOGOLEWSKI, S., ALINI, M. & WIMMER, M. A. 2006. Effects of simple and complex motion patterns on gene expression of chondrocytes seeded in 3D scaffolds. *Tissue Engineering,* 12**,** 3171-3179.

GUILAK, F. & MOW, V. C. 2000. The mechanical environment of the chondrocyte: a biphasic finite element model of cell–matrix interactions in articular cartilage. *Journal of Biomechanics,* 33**,** 1663-1673.

HEATH, C. A. & MAGARI, S. R. 1996. Mini-review: Mechanical factors affecting cartilage regeneration in vitro. *Biotechnology and Bioengineering,* 50**,** 430-437.

HUANG, C. Y. C., HAGAR, K. L., FROST, L. E., SUN, Y. & CHEUNG, H. S. 2004. Effects of Cyclic Compressive Loading on Chondrogenesis of Rabbit Bone-Marrow Derived Mesenchymal Stem Cells. *STEM CELLS,* 22**,** 313-323.

JUNG, Y., KIM, S. H., KIM, S. H., KIM, Y. H., XIE, J., MATSUDA, T. & MIN, B. G. 2008. Cartilaginous tissue formation using a mechano-active scaffold and dynamic

compressive stimulation. *Journal of Biomaterials Science, Polymer Edition,* 19**,** 61-74.

KIM, B., LEE, S., LEE, J., CHO, S., PARK, H., YEOM, S. & PARK, S. 2012. A comparison among Neo-Hookean model, Mooney-Rivlin model, and Ogden model for chloroprene rubber. *International Journal of Precision Engineering and Manufacturing,* 13**,** 759-764.

KOKKONEN, H. T., JURVELIN, J. S., TIITU, V. & TÖYRÄS, J. 2011a. Detection of mechanical injury of articular cartilage using contrast enhanced computed tomography. *Osteoarthritis and Cartilage,* 19**,** 295-301.

KOKKONEN, H. T., MÄKELÄ, J., KULMALA, K. A. M., RIEPPO, L., JURVELIN, J. S., TIITU, V., KARJALAINEN, H. M., KORHONEN, R. K., KOVANEN, V. & TÖYRÄS, J. 2011b. Computed tomography detects changes in contrast agent diffusion after collagen cross-linking typical to natural aging of articular cartilage. *Osteoarthritis and Cartilage,* 19**,** 1190-1198.

KULMALA, K. A. M., KORHONEN, R. K., JULKUNEN, P., JURVELIN, J. S., QUINN, T. M., KRÖGER, H. & TÖYRÄS, J. 2010. Diffusion coefficients of articular cartilage for different CT and MRI contrast agents. *Medical Engineering and Physics,* 32**,** 878-882.

LAI, W. M., MOW, V. C. & ZHU, W. 1993. Constitutive modeling of articular cartilage and biomacromolecular solutions. *Journal of Biomechanical Engineering,* 115**,** 474-480.

MAUCK, R. L., HUNG, C. T. & ATESHIAN, G. A. 2003. Modeling of Neutral Solute Transport in a Dynamically Loaded Porous Permeable Gel: Implications for Articular Cartilage Biosynthesis and Tissue Engineering. *Journal of Biomechanical Engineering,* 125**,** 602-614.

MAUCK, R. L., SOLTZ, M. A., WANG, C. C. B., WONG, D. D., CHAO, P. H. G., VALHMU, W. B., HUNG, C. T. & ATESHIAN, G. A. 2000. Functional tissue engineering of articular cartilage through dynamic loading of chondrocyte-seeded agarose gels. *Journal of Biomechanical Engineering,* 122**,** 252-260.

MOW, V. C., HOLMES, M. H. & LAI, W. M. 1984. Fluid transport and mechanical properties of articular cartilage: A review. *Journal of Biomechanics,* 17**,** 377-394.

MOW, V. C., RATCLIFFE, A. & ROBIN POOLE, A. 1992. Cartilage and diarthrodial joints as paradigms for hierarchical materials and structures. *Biomaterials,* 13**,** 67-97.

PEARLE, A. D., WARREN, R. F. & RODEO, S. A. 2005. Basic science of articular cartilage and osteoarthritis. *Clin Sports Med,* 24**,** 1-12.

POOLE, A. C. 1997. Articular cartilage chondrons: form, function and failure. *Journal of Cell Science,* 191**,** 1-13.

POOLE C. A, A. S., T. GILBERT R 1992. Chondrons from articular cartilage V.* Immunohistochemical evaluation of type VI collagen organisation in isolated

chondrons by light, confocal and electron microscopy. *Journal of Cell Science,* 103**,** 1101-1110.

POPP, J. R., ROBERTS, J. J., GALLAGHER, D. V., ANSETH, K. S., BRYANT, S. J. & QUINN, T. P. 2012. An Instrumented Bioreactor for Mechanical Stimulation and Real-Time, Nondestructive Evaluation of Engineered Cartilage Tissue. *Journal of Medical Devices,* 6**,** 021006-021006.

QUINN, T. M., MOREL, V. & MEISTER, J. J. 2001. Static compression of articular cartilage can reduce solute diffusivity and partitioning: implications for the chondrocyte biological response. *Journal of Biomechanics,* 34**,** 1463-1469.

SCHULZ, R. M. & BADER, A. 2007. Cartilage tissue engineering and bioreactor systems for the cultivation and stimulation of chondrocytes. *Eur Biophys J,* 36**,** 539-68.

SOPHIA FOX, A. J., BEDI, A. & RODEO, S. A. 2009. The basic science of articular cartilage: structure, composition, and function. *Sports Health,* 1**,** 461-8.

VALHMU, W. B., STAZZONE, E. J., BACHRACH, N. M., SAED-NEJAD, F., FISCHER, S. G., MOW, V. C. & RATCLIFFE, A. 1998. Load-controlled compression of articular cartilage induces a transient stimulation of aggrecan gene expression. *Archives of Biochemistry and Biophysics,* 353**,** 29-36.

WERNIKE, E., LI, Z., ALINI, M. & GRAD, S. 2008. Effect of reduced oxygen tension and long-term mechanical stimulation on chondrocyte-polymer constructs. *Cell and Tissue Research,* 331**,** 473-483.

WONG, M., WUETHRICH, P., BUSCHMANN, M. D., EGGLI, P. & HUNZIKER, E. 1997. Chondrocyte biosynthesis correlates with local tissue strain in statically compressed adult articular cartilage. *Journal of Orthopaedic Research,* 15**,** 189-196.

APPENDIX A

Static Seal for the lower chamber in the holder's reservoir

As illustrated below the parts consisting a static seal are an O-ring, a rod and a groove properly patterned in the bore.

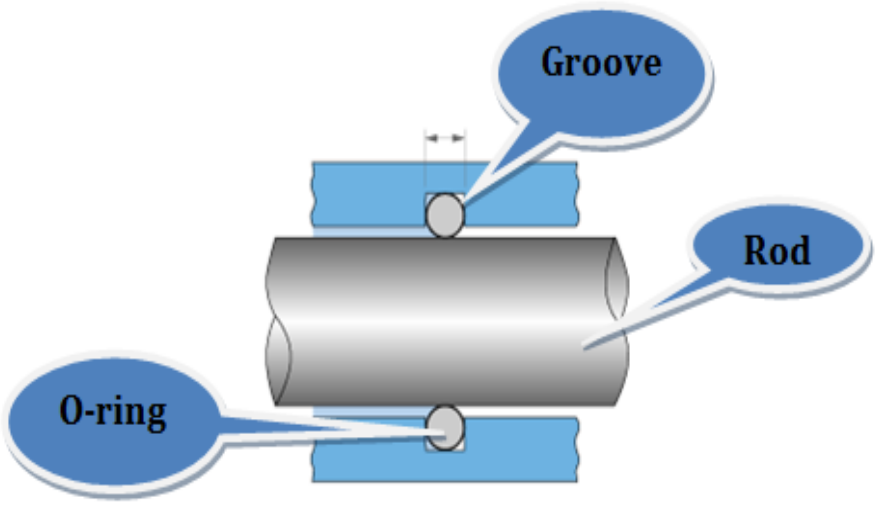

A Ø4mm leakage preventing rod was chosen for the specific application. When designing a static seal and a seal in general, determining the groove diameter is crucial for the performance of the seal. Depending on the seal type, i.e. static or dynamic, specific requirements do exist that ensure the optimum performance of the components, which are listed as follows:

- ✓ $O-ring\ compression\ squeeze = \frac{CS-H}{CS} * 100, where\ H\ is\ the\ groove\ depth$

For a static seal, the compression squeeze should be within 11% and 27%. Given that the cross-section of the O-ring is 1.8mm, the first step was to determine an acceptable depth range based on the aforementioned limits. Therefore, for each value the calculations were as follows:

$$\frac{CS - H_1}{1.8} = 0.11 \rightarrow H_1 = 1.602mm$$
$$\frac{CS - H_2}{1.8} = 0.27 \rightarrow H_2 = 1.314mm$$

In order to get the allowable range for the groove diameter, the formula that estimates the groove depth as a function of the groove diameter and the diameter of the rod was employed:

$$Depth = \frac{Groove - Rod}{2} \rightarrow H_1 = 1.602mm \rightarrow Groove_1 = 7.204mm$$
$$Depth = \frac{Groove - Rod}{2} \rightarrow H_2 = 1.314mm \rightarrow Groove_2 = 6.628mm$$

Therefore, a diameter equal to 7mm was chosen, which resulted in a grove depth equal to 1.5mm; based on those two values, the O-ring compression accounted for 16.67%. Next to that, the amount of groove filling is another parameter that needs to be estimates, and it is also found within specific limits in order to ensure satisfactory performance of the seal.

Groove filling is defined as follows:

- ✓ $Groove\ filling\ (\%) = \frac{\pi(\frac{CS}{2})^2}{wH}, where\ w\ the\ width\ of\ the\ groove$

Groove filling, is a parameter that indicates whether there is enough free space in the groove, in case of a possible expansion of the O-ring. The minimum and maximum recommended values for gland filling are 65% and 85%. For our design, the chosen parameters result in a groove filling equal to 70.65% that is found among the recommended range and ensures therefore the feasibility of the static seal.

APPENDIX B

Stability of Holder plate-Cartilage holder joint

As described on the Design chapter, the holder plate and the cartilage holder were kept together by means of 2M4X16 Nylon Slotted screws. In order to ensure the stability of the design a number of parameters had to be taken into account and they are presented as follows:

- ✓ *Minimum thread engagement length,* or in other words the axial distance over which an external thread is in contact with an internal thread. The Length of engagement should be big enough in order to ensure that in case of joint overload, the bolt will rather break than strip the threads of the tapered hole. The reason for taking that decision is that replacing a broken bolt is much easier and cost-effective than replacing a part with the tapered hole.

Assuming that the female and the male thread materials are the same, the minimum thread engagement length is given from the formula:

$$Le = \frac{(D - 0.938194)^2}{D - 0.64952 \times p}, where:$$

- $D, the\ basic\ diameter\ for\ the\ bolt$
- $p, the\ pitch\ distance\ for\ the\ thread$

On the other hand, if the male thread material is stronger than the female thread material, the length of engagement should be increased by a factor J, which is defined as:

$$J = \frac{Tensile\ strength\ of\ male\ thread}{Tensile\ strength\ of\ female\ thread}$$

Thus, the final minimum length of engagement for different male and female thread materials is given by the following formula:

$$Le_1 = Le \times J.$$

For our design D=4mm and p=0.7mm, and therefore Le=2.64mm. Additionally, the tensile strength of Rigid PVC and Nylon 6.6 resin are 65MPa and 165MPa respectively. Therefore, the factor J was estimated equal to 2.54. Accordingly, the final minimum length of engagement was calculated equal to 6.71mm. Thus, M4x16 screws are a good choice for the particular purpose, from the perspective of minimum engagement length.

- ✓ *Preload calculation,* i.e. the force that holds the joint together. Preload force, should be as high as possible, since it increases the strength of the joint, it generates friction between the parts to resist shear and improves the fatigue resistance of the bolted connections. For reusable connections, the preload is given by the following formula:

$$F_i = 0.75 \times A_b \times \sigma_P, where:$$

- $A_b = \frac{\pi}{16}(d_p + d_r)^2, the\ tensile\ area\ stress\ of\ the\ screw$
- $\sigma_P = 0.85 \times \sigma_y,\ the\ proof\ strength\ of\ the\ screw$

For ISO threads, d_p and d_r are defined as:

- $d_p = d - 0.64951p$
- $d_r = d - 1.226869p$

Based on the previous expressions A_b was found equal to 8.77mm^2. Next to that, given that the yield strength of 6.6 Nylon resin corresponds to 82.7MPa, the preload that should be applied on the screw was calculated and was found equal to 462.9N.

- ✓ *Separation of the joint*, or in other words the load which is required in order to make the joint loose and separate the flanges from each other. The separation load is a function of the preload and it can be estimated as follows:

$$W_{sep} = \left(1 + \frac{K_b}{K_c}\right) \times Preload, \text{where:}$$

- K_b, *is the stiffness of the clamping component, i.e. screw*
- K_c, *is the total stiffness of the clamped members*

The screw stiffness is calculated as follows:

$$K_b = \frac{A_b \times E_b}{l_b}, where:$$

- A_b *the tensile stress area of the scew*
- $E_{b,}$ *the modulus of elasticity of the screw material*
- l_b, *the screw length*

Therefore, the screw stiffness was estimated equal to 1437.73N/mm. As far as the stiffness of the clamped components is concerned, i.e. the holder plate and the cartilage holder, it was calculated based on their effective area. The effective area of those parts was calculated with the 30^0 cone angle technique, a technique that is well established in industry. The mathematical expression that is implemented for calculating the stiffness of the members is given below:

$$K = \frac{0.574 \times \pi \times E \times d}{ln\frac{(1.55t + D - d)(D + d)}{(1.55t + D + d)(D - d)}}, where:$$

- t, *the thickness of each clamped part*
- $D = 1.5 \times d$

The thickness of each component was chosen to overlap with the threaded length of each part; therefore for the holder plate t was assumed equal to 3.6mm, while for the cartilage holder it was assumed equal to 12.40mm. Accordingly the stiffness of each component was found equal to K_{C1}=29164.63N/mm and K_{C2} =23897N/mm respectively. Thereafter, the two components were assumed as two springs in series in order to determine the total stiffness, as follows:

$$K_{C=}\frac{K_{C1} \times K_{C2}}{K_{C1} + K_{C2}} = 13134{,}67 N/mm$$

Based on the previous calculations, the force required to separate the joint was found equal to 513.57N.

In this point, it should be emphasized that in order to achieve the recommended preload levels, any manual approach should be avoided; on the contrary the use of a torque wrench is recommended in order to apply the preload as precisely as possible. Due to the fact that we didn't possess such an instrument, the components were clamped manually; therefore it is obvious that this preload level was not possible to be accurately achieved. However, upon service no separation issues were observed, something that indicated the stability of the joint despite the absence of an accurate coupling instrument.

Stability of Indenter-Connector Joint

As illustrated in the drawing, the indenter is coupled with the connector through a M4X10 head-slotted screw. The procedure followed for this joint is almost identical to the previous one for the cartilage holder-holder plate joint; the only difference is the material of the indenter (Acrylate, tensile strength=70MPa, E=3200MPa). The minimum thread engagement length is again calculated based on the softest material, due to the fact that it appears to be more prone to strip in case of overloading. The calculation was again performed based on the material properties of Rigid PVC, and the minimum thread engagement length was found equal to 6.71mm.

With respect to the separation load, this time the thickness of each part was again assumed to correspond to 3.60mm for the connector and 6.4mm for the indenter. The stiffness for the indenter and the connector were 35406.604N/mm and 26927.689N/mm for the indenter and the connector respectively. Like before, the total stiffness was estimated equal to 15295.241N/mm, and given that the recommended preload was again equal with 462.9N, the separation load corresponded to 506.4N.

Stability of Rod-Connector Joint

Based on the aforementioned procedure, the minimum thread engagement length is calculated based on D and p. For M3 ISO threads p is equal to 0.5mm. The minimum thread engagement length was therefore equal to 1.58mm. Similarly to holder plate-cartilage holder system, the increase factor J was equal to 2.54mm and therefore the thread engagement length required for the stability of the joint corresponded to 4.01mm. For the preload, again the same formula was implemented; the tensile stress area of the M3 screw was found equal to 5.04 mm^2 and therefore the required preload corresponded t0 265.7N.

For the separation load the stiffness of each component was calculated as described before. The calculations attributed the screw stiffness equal to 1652.48N/mm, while the stiffness for the rod and the connector were 13637.23N/mm and 14472.16N/mm respectively. The total stiffness was determined equal to 7021.06N/mm and the separation load was found equal to 328.1N.

APPENDIX C

Convergence study for the Diaphragm FEM in ABAQUS

The convergence study was performed by applying 0.1mm displacement to the model reference points, while changing the number of elements each time. The procedure was repeated until it was observed that the accuracy obtained for 188856 elements was slightly higher from the accuracy obtained for seeding the model with 107712 elements (0.3%). Therefore, it was concluded that for the sake of high accuracy but decreased computational cost at the same time, the simulations could be performed with the model being seeded with 107712 elements.

Number of Elements	Reaction force, RT3 (N)
3696	**2.671**
4368	**2.648**
5252	**2.630**
6612	**2.610**
8580	**2.590**
10728	**2.579**
31228	**1.831**
44096	**1.823**
107712	**1.654**
188856	**1.649**

APPENDIX D

Dimensional Stability of the plastic components involved in the compression unit

When polymers are subjected to constant load they gradually release strain, and this is the well-known creep phenomenon. Creep constitutes one of the main considerations when designing with plastics, since the dimensional stability is one of the most significant parameters to be considered. As stated in the Design chapter and illustrated in the following graph, rigid PVC is associated with a rather satisfying creep response, when compared with other polymers, and therefore it constituted a good choice as the fabrication material. As described before, the present device allows the performance of stress-relaxation tests in order to determine the material properties of the tested sample. Thus, it is necessary to ensure that when the desired displacement is prescribed, the components of the compression unit remain stable. The most crucial component, which ‘’carries’’ the applied displacement pattern is the connector. When the sample is loaded, the resulting reaction force is transmitted to the rest components and this is how it is finally detected by the load cell. Therefore, when the stress relaxation pattern causes the sample to reach the average maximum reaction force, the connector is loaded by this amount of force. For the extreme case, where the maximum reaction force during the applied stress relaxation patterns reaches the value of 45N (maximum loading capacity of the load cell), the connector is subjected to a compressive stress equal to 0.4MPa or $0.04 kg/mm^2$. Based on the graph below, these stress level result in quite small creep strain levels that potentially have a very small impact on the measurements performed with the particular custom-made device.

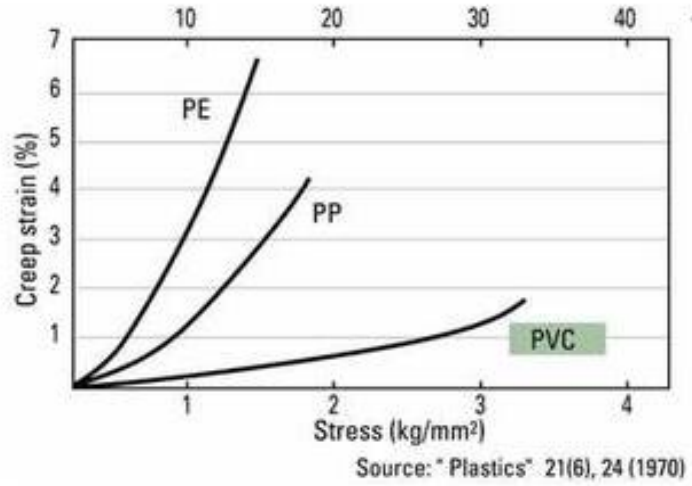

Apart from potential creep phenomena associated with the plastic components, their strain response when been subjected to the sample's reaction force had to be investigated. For simplification of the design analysis the nonlinear behavior of the plastic components was not taken into consideration; therefore the Hooke's law was employed for determining the potential components' displacement.

Like before, the maximum external force was assumed equal to 45, or in other words equal to the loading capacity of the load cell. Since the stability of the bolt joints was ensured through the previous preload-separation load calculations, the system indenter-connector-rod was considered one single rod of variable cross-section. Additionally, due to the fact that various components form the motion unit, the cross-sectional variation was not considered as uniform; therefore the displacement for each component was calculated and they were thereafter added in order to get an estimation of the total displacement. The process is described in detail as follows:

- Connector plus rod part in contact

$$\varepsilon_{con} = \frac{\sigma_{con}}{E} = \frac{F}{A_{con}E} = 0.005\%$$

$$disp_{con} = \varepsilon_{con} * l_{con+rod\,part} = 0.001mm$$

- Rod part not in contact with the connector

$$\varepsilon_{Rod} = \frac{\sigma_{Rod}}{E} = \frac{F}{A_{Rod}E} = 0.019\%$$

$$disp_{rod} = \varepsilon_{rod} * l_{rod} = 0.007$$

- Indenter

$$\varepsilon_{indenter} = \frac{\sigma_{indenter}}{E} = \frac{F}{A_{indenter}E} = 0.042\%$$

$$disp_{ind} = \varepsilon_{ind} * l_{ind} = 0.007$$

The previous calculations mean that for the extreme case that the unit will be subjected to an external load equal to 45N the total displacement of the components would correspond to 0.015mm. As stated in the previous chapter, the recommended displacement of the unit in order to reach subject a sample to 10% compression without overstretching the membrane at the same time was set equal to 1.1mm. Therefore, the displacement of the components attributes to a total discrepancy of 1.36% when a displacement of 1.1mm is applied. However, the tissues that are supposed to be tested with this device are way softer and therefore the expected reaction force levels do not exceed 25N. Thus for the specific tissue samples, the observed discrepancy due to the incorporation of plastic components drops well below 1%; therefore there is a small impact on the measuring capabilities of the device owing to the dimensional stability of the plastic components.